AD-A096 795 TEXAS UNIV AT AUSTIN DEPT OF AEROSPACE ENGINEERING AN--ETC F/G 20/4
THE ANALYSIS OF SECONDARY FLOWS FOR TUBE-LAUNCHED ROCKET CONFIG--ETC(U)
JAN 81 H H KORST, J J BERTIN DAAH01-80-C-0118
UNCLASSIFIED 81001 DRSMI/RL-CR-81-3 NL

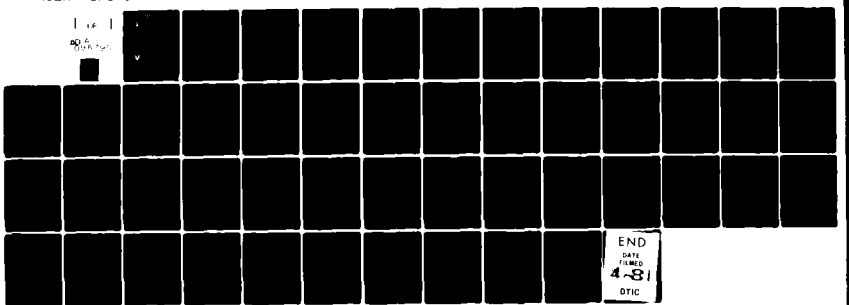

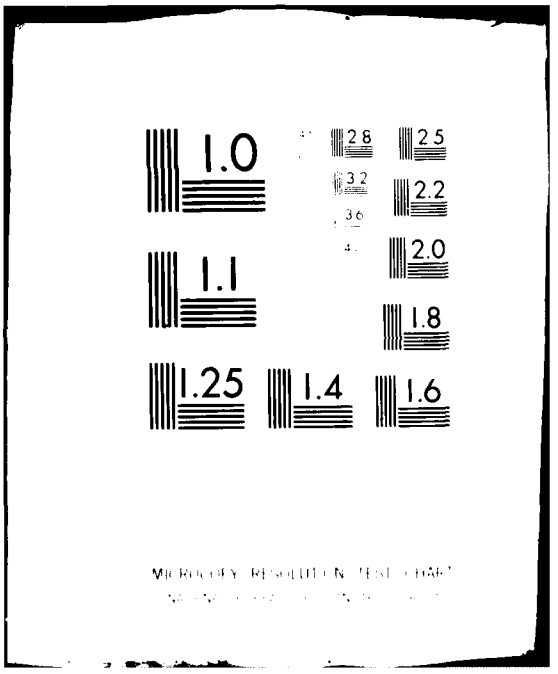
1.0
2.8
2.5
3.2
2.2
3.6
2.0
1.1
1.8
1.25
1.4
1.6

(2) LEVEL III

TECHNICAL REPORT TR-RL-CR-81-3

THE ANALYSIS OF SECONDARY FLOWS FOR TUBE-LAUNCHED ROCKET CONFIGURATIONS

by

H. H. KORST
Department of Mechanical and Industrial Engineering
The University of Illinois at Urbana-Champaign

and

John J. Bertin
Department of Aerospace Engineering and Engineering Mechanics
The University of Texas at Austin

This research was supported through Grant DAAG-29-76-G-0209 and Contract DAAH01-80-C-0118

U.S. ARMY MISSILE COMMAND
Redstone Arsenal, Alabama 35898

15 January 1981

Approved for Public Release
Distribution Unlimited

DISPOSITION INSTRUCTIONS

Destroy this report when it is no longer needed. Do not return it to the originator.

DISCLAIMER

The findings in this report are not to be construed as an official Department of the Army position unless so designated by other authorized documents.

TRADE NAMES

Use of trade names or manufacturers in this report does not constitute an official indorsement or approval of the use of such commercial hardware or software.

SECURITY CLASSIFICATION OF THIS PAGE *(When Data Entered)*

REPORT DOCUMENTATION PAGE

READ INSTRUCTIONS BEFORE COMPLETING FORM

1. REPORT NUMBER: Technical Report TR-RL-CR-81-3
2. GOVT ACCESSION NO.: AD-A096
3. RECIPIENT'S CATALOG NUMBER: 795

4. TITLE *(and Subtitle)*: THE ANALYSIS OF SECONDARY FLOWS FOR TUBE-LAUNCHED ROCKET CONFIGURATIONS

5. TYPE OF REPORT & PERIOD COVERED: Final on phase 1 Oct. 1979 - 30 Nov. 1980

6. PERFORMING ORG. REPORT NUMBER:

7. AUTHOR(s): H. H. Korst, John J. Bertin

8. CONTRACT OR GRANT NUMBER(s): DAAH01-80-C-0118

9. PERFORMING ORGANIZATION NAME AND ADDRESS: Department of Aerospace Engineering and Engineering Mechanics, The University of Texas at Austin, Austin, Texas 78712

10. PROGRAM ELEMENT, PROJECT, TASK AREA & WORK UNIT NUMBERS:

11. CONTROLLING OFFICE NAME AND ADDRESS: Commander, US Army Missile Command, Attn: DRSMI-RPT, Redstone Arsenal, AL 35898

12. REPORT DATE: 15 January 1981

13. NUMBER OF PAGES:

14. MONITORING AGENCY NAME & ADDRESS *(if different from Controlling Office)*: Commander, US Army Missile Command, Attn: DRSMI-RLH, Redstone Arsenal, AL 35898

15. SECURITY CLASS. *(of this report)*: Unclassified

15a. DECLASSIFICATION/DOWNGRADING SCHEDULE:

16. DISTRIBUTION STATEMENT *(of this Report)*: Approved for public release; distribution unlimited

17. DISTRIBUTION STATEMENT *(of the abstract entered in Block 20, if different from Report)*:

18. SUPPLEMENTARY NOTES: The findings of this report are not to be construed as an official Department of the Army position unless so designated by other authorized documents.

19. KEY WORDS *(Continue on reverse side if necessary and identify by block number)*: Free-Flight Rockets; Mallaunch of Free Rockets; Launch Tube Flow Fields

20. ABSTRACT *(Continue on reverse side if necessary and identify by block number)*:

Theoretical flow-fields have been calculated for various nozzle/launch-tube configurations using this flow model. The solutions, thus calculated, are compared with experimental data in the present paper. The principal objectives of the present paper are (1) to present an engineering model for the impingement flow-field which is produced when an underexpanded supersonic nozzle is exhausted into a constant-area tube, (2) to compare the computed flow-field solutions with experimental results, and (3) to use the comparisons to establish the validity of the flow model.

DD FORM 1 JAN 73 1473 EDITION OF 1 NOV 65 IS OBSOLETE

SECURITY CLASSIFICATION OF THIS PAGE *(When Data Entered)*

THE ANALYSIS OF SECONDARY FLOWS FOR TUBE-LAUNCHED ROCKET CONFIGURATIONS*

by

H.H. Korst
University of Illinois

and

John J. Bertin
The University of Texas

Aerospace Engineering Report 81001

*This work was supported by the U.S. Army Missile Command through Grant DAAG-29-76-G-0209 and Contract DAAH01-80-C-0118

The University of Texas at Austin

January 1981

THE ANALYSIS OF SECONDARY FLOWS FOR TUBE-LAUNCHED ROCKET CONFIGURATIONS*

by

H.H. Korst
Professor, Department of Mechanical and
Industrial Engineering
University of Illinois at Urbana-Champaign

and

John J. Bertin
Professor, Department of Aerospace Engineering
and Engineering Mechanics
The University of Texas at Austin

*The individual research efforts discussed herein were supported by the U.S. Army Research Office through Grant DAAG-29-76-G-0209 and by the U.S. Army Missile Command through Contract DAAH01-80-C-0118

TABLE OF CONTENTS

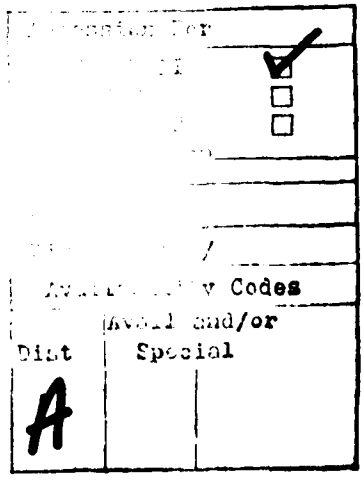

Introduction

Various military rockets are launched from tubes. The designer of a tube-launched rocket system must consider the possibility of unbalanced forces acting on the rocket that are caused by flow in the annular gap between the rocket and the launcher wall. As the underexpanded nozzle flow accelerates upon leaving the nozzle, it entrains air from the annular gap forming a shear layer at the plume boundary. The exhaust plume impinges on the wall a short distance downstream of the nozzle exit-plane, creating an impingement shock-wave. When the impingement shock-wave is very weak, a fraction of the entrained air has been given sufficient momentum so that it passes through the impingement shock and the system acts as an ejector. Using the atmosphere at the upstream end of the launcher as its source, a low velocity flow develops in the annular regions to supply the mass flow-rate of air that is carried through the shock wave. A fraction of the air entrained by the exhaust plume does not gain sufficient momentum to pass through the shock wave and is turned upstream, creating a separation "bubble" near the launcher wall. Thus, as indicated in the sketch of Fig. 1a, the discriminating streamline can be traced into the annular region between the rocket and the launcher wall.

If the stagnation pressure is increased above the values for ejector-type flow or if the nozzle exit-angle is relatively large, the flow at the plume boundary must turn through a larger angle when it encounters the wall. Thus, although classified as a weak solution, the pressure rise across the shock wave increases. Once the impingement shock-wave becomes sufficiently strong, the resultant adverse pressure gradients causes a fraction of the exhaust flow to be turned upstream into the annular gap, as shown in Fig. 1b. The exhaust that is turned upstream is known as blow-by flow.

When conditions are such that the impingement shock-wave system is strong, massive blow-by occurs. The essential elements of a flow model for this launch-tube flow field have been identified experimentally[1]. A one-dimensional, theoretical, flow-model, which correlates well with the

experimental data, has been developed[2]. The pressure gradients and asymmetries resulting from turning a large fraction of the exhaust flow upstream into the annular gap cause unbalanced forces on the rocket. Because the rocket is flying free in the launch tube at this time, these forces can cause the rocket to deviate significantly from its intended flight path. Such deviations in the rocket's trajectory have been observed in flight tests[3] and in cold-gas simulations[4,5]. Therefore, although it is necessary to understand launch-tube flow fields with massive blow-by, they should be avoided whenever possible.

To predict the magnitude and the direction of the flow in the annular gap, one must be able to describe the exhaust plume of the rocket and the viscous/shock-interaction structure that results when the plume encounters the launcher wall. The strength of the impingement shock wave and the characteristics of the viscous interaction at the wall depend on the structure of the exhaust plume and on the geometry of the launch tube. When an underexpanded, supersonic nozzle exhausts into a constant-area tube, the strength of the impingement shock-wave depends on the Mach number of the inviscid flow along the inner edge of the mixing zone at the jet boundary, on the ratio of the specific heats (γ), on the inclination of the impinging flow relative to the launcher wall, and on the velocity profile in the mixing zone.

For a wide range of test conditions, the impingement shock-wave is relatively weak and the downstream flow remains supersonic. For such cases, there is relatively little secondary flow and the pressure in the annular region differs only slightly from the atmospheric value. As a result, unbalanced forces on the missile are relatively small. The Chapman-Korst model[6] can be used to delineate the inviscid and the viscid flow-mechanisms encountered in the plume-impingement flow-field. Once the geometry of the corresponding inviscid plume-boundary is established by an appropriate potential flow analysis, a viscous mixing component is superimposed on the boundary. Wake closure conditions are specified in the form of a modified concept of incomplete turning of the plume near the point of shear-layer reattachment[7].

Theoretical flow-fields have been calculated for various nozzle/

launch-tube configuration using this flow model. The solutions, thus calculated, are compared with experimental data in the present paper. The principal objectives of the present paper are (1) to present an engineering model for the impingement flow-field which is produced when an underexpanded supersonic nozzle is exhausted into a constant-area tube, (2) to compare the computed flow-field solutions with experimental results, and (3) to use the comparisons to establish the validity of the flow model.

Nomenclature

A	Cross-section
C	Crocco number
d	Diameter
M	Mach number
$\dot{m}$	Mass flow-rate
p	Pressure
r	Radius, measured perpendicular to the centerline of the launch tube
R_1	Initial radius of curvature of the inviscid plume boundary
T	Temperature
u	Streamwise velocity component
x	Axial distance along the centerline of the launch tube or streamwise distance (arc length) along the inviscid plume boundary
y	Normal distance to the inviscid plume boundary
γ	Ratio of specific heats
η	Nondimensional shear-layer coordinate
θ	Flow inclination relative to the centerline of the launch tube
σ	Spreading parameter, defined by equation (1)
ϕ	Dimensionless velocity ratio
ω	Prandtl-Meyer angle

Subscripts

ag	Denotes static properties evaluated at the upstream end of the annular gap
b	Denotes static properties in the base region
d	Discriminating (dividing or stagnating) streamline
ex	Flow through the nozzle exit-plane, i.e., the exhaust flow
F	Free-jet surface (inviscid plume boundary)
i	Denotes properties evaluated at the intersection of the inviscid plume boundary and the launcher wall
j	Zero streamline, i.e., that dividing the exhaust flow from the base air
L	Denotes local conditions at the lip of the nozzle exit-plane
ne	Denotes properties evaluated in the nozzle exit-plane

Subscripts (cont.)

pit	Pressure measured using a pitot probe collinear with the launcher-tube axis
pk	Denotes peak values
r	Outer surface of the rocket
t	Inner surface of the launch tube
t1	Denotes properties evaluated in the stagnation chamber of the simulated rocket
t2	Denotes properties downstream of a normal shock wave
v	Beginning of viscous interaction
1	Mass flow-rate given by equation (6)

Theoretical Analysis

A component approach for supersonic, turbulent flows, i.e., the Chapman-Korst model[6], forms the basis for the present analysis. It includes the delineation of inviscid and viscid flow-mechanisms encountered in plume/launcher-wall impingement flows and their subsequent synthesis into an overall systems solution. The geometry of the corresponding inviscid plume boundary is established by an appropriate potential flow analysis. The viscous mixing component is superimposed on this boundary. Wake closure conditions are specified in the form of a modified concept of the incomplete turning of the plume near the point of shear layer reattachment[7]. A number of conceptual simplifications for the plume-impingement flow field, which will be introduced, are justifiable for the conditions of interest.

Since the launching of rockets from straight tubes will generally impose geometric restrictions to blow-by, the present analysis can be simplified by the assumption that the mass flow-rates which will be rejected from or entrained into the viscous jet mixing region should be small. This, in turn, allows the adoption of a linear velocity profile in the mixing region[8]. It is assumed that the entire system will be operating under essentially isoenergetic conditions, that is, with the stagnation temperature equal to that of the exhaust gas. This assumption is realistic for most flows under consideration; the exception being ejector-type flow generated by an actual rocket firing.

Since the ratio of the launch-tube diameter to rocket nozzle-exit diameter is limited to values ≤ 1.5, the contour of the corresponding inviscid plume boundary can be determined with sufficient accuracy by the second-order potential-flow approximation for axially symmetric, supersonic flow near the center of an expansion[9,10]. The resulting circular-arc configuration is convenient for establishing a simple inviscid-flow-component geometry. On the other hand, it is necessary to treat the nozzle flow in detail in order to define accurately the conditions at, and near, the lip of the exit cross-section. This requires the analysis of the nozzle flow by the method of characteristics (including the effects of characteristics coalescence) as it develops from the transonic flow region

near the nozzle throat[11].

The exit-plane conditions near the nozzle lip, will be determined by the local wall-slope, θ_L, the local wall-curvature, the local Mach number, M_L, and the local flow acceleration. With these initial conditions specified, selection of the jet surface Mach number, M_F, will yield a unique solution for the circular-arc approximation of the contour of the inviscid plume boundary in terms of the initial streamline angle, θ_F, and the radius of curvature, R_1[12].

Thus, for a given nozzle configuration and for any jet surface Mach number, M_F, the inviscid flow field will be uniquely determined, see Fig. 2, with θ_i denoting the inviscid impingement angle at the cylindrical launcher wall, i.e., at radius r_t. One now has to analyze the viscous flow mechanisms which will provide the closure conditions for determining the actual operating condition of the system.

As mentioned above, the jet mixing characteristics of the free shear-layer at the plume boundary can be approximated by selecting isoenergetic conditions and a linear velocity profile*. The spread parameter σ shall here be related to the rate of change in slope of the velocity profile[14,15] in the form:

$$\sigma = \frac{\sqrt{\pi}}{u_F} \quad \frac{1}{\frac{\partial}{\partial x}\left[\left(\frac{\partial u}{\partial y}\right)_{max}\right]} \tag{1}$$

For a linear velocity profile with the conditions at the "inviscid" plume boundary given by u_F and ρ_F, one finds:

$$\phi = \frac{u}{u_F} = \frac{\eta}{\sqrt{\pi}} \tag{2}$$

where $\eta = \sigma \frac{y}{x}$. The density ratio in the iso-energetic mixing region is:

---

*Use of a self-similar, linear mixing profile does not exclude the study of Reynolds number effects. The effects of the boundary layer along the nozzle wall can be considered, subsequently either in form of an equivalent bleed[7,13] or by analyzing the development of a dissipative shear layer in a rotational but essentially non-dissipative flow field envisioned by the flow expansions near the nozzle lip.

$$\frac{\rho}{\rho_F} = \frac{1 - C_F^2}{1 - \phi^2 C_F^2} \tag{3}$$

where use of the Crocco number,

$$C_F = M_F \sqrt{\frac{2}{\gamma - 1} + M_F^2}\ , \tag{4}$$

conveniently eliminates the influence of the specific heat ratio on constant-pressure mixing profiles.

Application of the momentum equation to a two-dimensional mixing region allows one to locate the profile with respect to the corresponding inviscid jet boundary in the form:

$$\eta_M = \sigma \frac{y_M}{x} = \sqrt{\pi} \left\{ 1 - \left(\frac{1 - C^2}{C^2} \right) \left(-1 + \frac{1}{2C} \ln \left(\frac{1 + C}{1 - C} \right) \right) \right\} \tag{5}$$

One should note that the application to an axisymmetric, curved plume boundary requires that the length be interpreted as an arc length and that the use of σ values originally defined for planar mixing zones adds to the inherent uncertainty in making an assessment for the effects of compressibility on the spread parameter. For the present purpose, where the Mach number range for M_F will seldom exceed 3.5, one may use the simple relationship[16]:

$$\sigma = 12 + 2.56\ M_F$$

The mass rate of flow per unit depth within the mixing zone up to the streamline y:

$$\dot{m}_1 = \int_{y \to -\infty}^{y(\phi)} \rho u\, dy$$

can now be expressed in closed form by:

$$\dot{m}_1 = I_1(\phi, C_F)\ \frac{x\ u_F\ \rho_F}{\sigma} \tag{6}$$

where $I_1(\phi,C_F) = \sqrt{\pi}\ \dfrac{\left(C_F^2 - 1\right)}{2C_F^2}\ \ln\left(1 - \phi^2 C_F^2\right)$; (6a)

the velocity ratio $\phi = \dfrac{u}{u_F}$ defines a streamline having the location $y = \dfrac{x}{\sigma}\left(\eta_M - \dfrac{\phi}{\sqrt{\pi}}\right)$ measured perpendicular to and outside of the corresponding inviscid plume boundary. The velocity along the zero streamline, which separates the nozzle flow from the air entrained from the base region is given by

$$\phi_j = \frac{1}{C_F}\sqrt{1 - \left(1 - C_F^2\right)\ \text{EXP}\left[\frac{1}{C_F}\ln\left(\frac{1 + C_F}{1 - C_F}\right) - 2\right]} \tag{7}$$

The recompression of the plume as it impinges on the cylindrical wall leads to a flow configuration as shown in Fig. 2b. If the stagnating (discriminating) streamline has a velocity level, ϕ_d, different from that of the zero streamline, ϕ_j, a secondary flow will be established as required for satisfying the conservation of mass in the near wake region. The secondary flow rate will be positive, i.e., ejector-type flow, if $\phi_j > \phi_d$ and negative, i.e., blow-by, if $\phi_j < \phi_d$. The secondary flow rate may be approximated as

$$\dot{m} = 2\pi r_t \frac{x}{\sigma} u_F \rho_F [I_1(\phi_j,C_F) - I_1(\phi_d,C_F)] \tag{8}$$

The condition $\phi_j = \phi_d$ corresponds to an operation without any secondary flow which will be satisfied for near wake vented to the atmosphere if

$$\left.\frac{p}{p_{t1}}\right|_{M_F} = \frac{p_{atm}}{p_{t1}}$$

or the case where the annular gap is isolated by a tight fitting sabot or by an obturator ring.

As the discriminating streamline, whose velocity ratio is ϕ_d, stagnates at the wall, the process of recompression will be practically isentropic[6,7]. Hence, for a local wall pressure corresponding to an inviscid value of

the Crocco number, $C_d = C_F \phi_d$,

$$\phi_d = \frac{1}{C_F} \sqrt{\frac{C_F^2 - C_d^2}{1 - C_d^2}} \quad . \tag{9}$$

Since the reattachment point of this streamline falls into a region where the adjacent inviscid plume flow-field has not yet fully aligned with the solid wall, the concept of an incomplete turning angle will be utilized.

For a linear velocity profile, the correlation proposed by Page, et al.[17] for cases involving mass bleed reduces to a remarkably simple expression:

$$A = \frac{\omega(C_F) - \omega(C_d)}{\omega(C_F) - \omega(C_i)} = 0.59 \tag{10}$$

which is valid over a range of inviscid boundary Mach number from 1 to 5, i.e. $1 \leq M_F \leq 5$. In equation (10), $\omega(C)$ is the Prandtl-Meyer function (which depends on the Crocco number) and C_i is the Crocco number for the inviscid flow after the impingement of the inviscid jet and its realignment with the launcher wall.

Equations 1 through 10 can be solved to establish the theoretical operating conditions using information about the base pressure, which is approximately equal to the atmospheric value when the annular gap is vented, and the peak reattachment pressure, which is located a distance:

$$x_i = R_1(\sin \theta_L - \sin \theta_i) \tag{11}$$

from the nozzle exit-plane. For cases where the secondary flow rates are large, equations 1 through 10 must be supplemented by a relationship between the mass flow-rate and the pressure drop in the annular gap. This additional relation for the large flow-rates in the annular gap is discussed in Ref. 2.

The inviscid pressure rise will start near the location, see Fig. 2b,

$$x_v = R_1 \left[\sin\theta_L - \sin\theta_v \left[1 + \left(\theta_L - \theta_v \right) \frac{\pi}{180} \frac{\eta_M}{\sigma} \right] \right] \tag{12}$$

where the implicit equation for θ_v

$$\theta_v = \cos^{-1}\left[\left(\cos\theta_i - \frac{(\theta_L - \theta_v)\sqrt{\pi}}{180\sigma}\phi_d\right)\Big/\left(1 + \frac{(\theta_L - \theta_v)\pi}{180\sigma}\eta_M\right)\right] \qquad (13)$$

has to be solved by iteration.

After plume impingement and alignment of the jet surface with the wall by reversible compression, the pressure distribution for the inviscid flow configuration can again be treated with reasonable approximation by the formal application of the concept of centered expansions. With the new origin of the centered expansion of the impingement point for the inviscid plume, an ordinary differential equation is obtained for M^* along the wall downstream of the impingement and the resulting pressure distribution can be determined. The mathematical approximations inherent in the method of centered expansions restricts the useful range of the calculated wall-pressure distribution to approximately 1.0 r_{ne} downstream of the impingement.

It is of interest to explore the influence of Reynolds number together with an assessment of the nozzle-wall boundary-layer development. The boundary layer in axisymmetric, convergent/divergent nozzles can be calculated[18,19,20] at the nozzle lip. Then, for a given Mach number, M_F, one can calculate the development of the dissipative shear layer following the expansion from the nozzle exit-plane. After the transition of the thin laminar sublayer[21], the turbulent mixing layer grows until its inner edge reaches and then crosses into the "free-stream" within the rotational shear layer produced by the expanded nozzle boundary layer. The developing mixing layer proceeds toward, but usually does not reach, self-similar mixing profiles. Calculations for the present test conditions indicate that the velocity along the dividing streamline is within five percent of the similarity value. Thus, the test simulations of the current program provide a reasonable simulation for the prototype reattachment pressure rise.

Of greater concern is the behavior of the reattaching flow due to the strong interaction with its boundary layer. Implied with the concept of incomplete turning of the adjacent inviscid stream is the continuation of the pressure rise beyond the stagnation point within the dissipative layer.

This will lead to a thickening of the attached boundary layer and may, by itself, cause a pressure overshoot above the level consistent with the full turning of the external flow.

On the other hand, there will also be a communication within the boundary layer of the rapid expansion following the plume impingement. These mechanisms are expected to modify the pressure distribution across the reattachment region, but in opposing fashion. As a result, pressure peaks determined for the corresponding inviscid jet boundary will generally show reasonable agreement with experimental data even though there may be noticeable, albeit explainable, differences between theoretically determined and measured pressure distributions.

Experimental Program

The experimental results presented in this paper were obtained at the Rocket Exhaust Effects Facility located at the Experimental Aerodynamics Laboratory (EAL) of the University of Texas at Austin. Simulated rocket exhaust plumes were obtained by accelerating unheated, compressed air (the test gas) through a convergent/divergent nozzle (the simulated rocket). The nozzle flow was exhausted either into quiescent air or into a constant-area launch tube. A sketch of a typical nozzle/launch-tube configuration is presented in Fig. 3. The simulated launch tubes were mounted on a moveable table, so that the location of the launch tube relative to the exit plane of the simulated rocket nozzle could be varied. For all of the runs in the present test program, the axis of the launch tube was collinear with the axis of the simulated rocket nozzle.

The test schedule included three different nozzle geometries and three launch tubes. Since the objective of the present paper is to use the experimental data to validate the theoretical flow model and to establish the limits of its validity, only selected data are presented in this paper. For a more complete discussion of the experimental programs, the reader is referred to refs. 22 and 23.

Simulated Rockets

Simulated rocket exhaust flows were produced by accelerating unheated air through convergent/divergent nozzles. Data are presented for two of the nozzle configurations,

1) a 20° conical convergent divergent nozzle, designated as C3, and
2) a 10° conical contoured convergent divergent nozzle, designated as C5.

The geometries of the nozzle configurations studied in the current program are presented in the equations below.

The 20° Conical Nozzle, C3:

For $-1.308 \leq x \leq -1.031$:

$$(x + 1.308)^2 + (r - 1.626)^2 = (0.813)^2$$

For $-1.031 \leq x \leq 0.0$:

$$r = 0.759 + 0.364\ (x + 1.308)$$

The 10° Contoured Nozzle, C5:

For $-2.908 \leq x \leq -1.895$:

$$(x + 2.098)^2 + (r - 1.626)^2 = (0.813)^2$$

For $-1.895 \leq x \leq 0.0$:

$$r^2 = 1.530 + 0.434x$$

The equations give the dimensions in centimeters. A sketch of the C5 nozzle is presented in Fig. 4. The throat radius, the nozzle exit-plane radius, and the external radius of the rocket were the same for all nozzles.

The cross-sectional area for all nozzle exit-planes was $A_{ne} = 2.316A^*$. If the acceleration of the flow through the nozzles of this area ratio were isentropic, the Mach number of the nozzle exit plane would be 2.36 (ref. 24).

Simulated Launch Tubes

The constant area launch tubes, designated as L1, L2, and L3, were used for the tests (Fig. 3). The inside radius (r_t) for the smooth bored tubes was 1.20 r_{ne} (1.484 cm) for the L1 configuration, 1.275 r_{ne} (1.522 cm) for the L2 configuration, and 1.50 r_{ne} (1.855 cm) for the L3 configuration. Static pressure orifices (0.0635 cm in diameter) were located axially along the tube wall at a spacing of 0.25 r_{ne} (0.309 cm). Additional static pressure orifices spaced 0.50 r_{ne} (0.618 cm) apart were located further downstream.

For each test configuration, i.e., nozzle/launch-tube configuration, two pitot-static probes were located midway between the simulated rocket and simulated launcher wall and 4.128 cm from the upstream end of the launch tube. Static pressure orifices were located in the launch-tube wall at the face of the pitot probes. These pitot-pressure/static-pressure data could be used to "measure" the mass flow-rate in the annular gap. The pitot probe was designed so that it could face either upstream or downstream in order to "measure" the mass flow-rate in either direction, i.e., ejector flow or blow-by flow.

The Mass Flow-Rate

The mass flow-rates were calculated using the pressure data from the pitot-static probes located at the upstream end of the annular gap. If one assumes one-dimensional, isentropic flow in the annular gap, and perfect gap properties, then the dimensionless mass flow-rate is given by:

$$\frac{\dot{m}_{ag}}{\dot{m}_{ex}} = M_{ag}\sqrt{\frac{T_{tl}}{T_{ag}}}\,\frac{p_{ag}}{p_{tl}}\left\{\frac{(r_t^2 - r_r^2)}{\sqrt{\frac{2}{\gamma+1}}\left[\frac{2}{\gamma+1}\right]^{\frac{1}{\gamma-1}}(r^*)^2}\right\} \qquad (1)$$

For those runs where blow-by occurred, p_{ag} was assumed to be the atmospheric value and the measured pitot pressures were used to calculate M_{ag}. For the ejector flow calculations, the pitot pressures were assumed to be the atmospheric value while the measured value of $\bar{p}_{ag}$ was used in the calculation of the Mach number in the annular gap.

Obturator Rings

For some of the runs, obturator rings were used to seal the base region so that there could be no flow in the annular gap. The obturator ring fit snugly into the annular gap at an x of approximately -1.270 cm i.e., upstream of the nozzle exit plane.

Discussion of Results

Solutions of the theoretical flow-fields have been computed from the transonic region of the nozzle throat, through the nozzle, and through the impingement of the jet-exhaust plume on the launcher-wall. Computed solutions have been obtained both for the C3 and for the C5 nozzles. Thus, the theoretical solutions of the rocket exhaust flow-field represent the effects of the actual nozzle geometries on the overall flow-field. The theoretical solutions will be compared with the experimental data. In some cases, two theoretical solutions representing varying degrees of rigor were generated. In such cases, the theoretical solutions will be compared with each other.

Nozzle Flow Field

The static pressures were measured along the wall of the divergent section of the C5 nozzle for stagnation pressures from 0.7×10^6 N/m^2 to 8.8×10^6 N/m^2. For stagnation pressures of 3.4×10^6 N/m^2, or greater, the values of the ratio p/p_{t1} were a function of position only. The non-dimensionalized static-wall-pressure measurements are compared in Fig. 5 with the theoretical values computed using the method of characteristics. The agreement between the theoretical and the experimental distributions is excellent.

The radial pitot-pressure distributions which result when unheated air is accelerated from a reservoir where p_{t1} is 8.715×10^6 N/m^2 through the C3 nozzle and exhausts into quiescent air are presented in Fig. 6. The theoretical values of p_{t2}/p_{t1} are compared with experimental pitot pressure for the nozzle exit-plane ($x = 0.0\ r_{ne}$) and for the plane at $x = 0.5\ r_{ne}$. Theoretical values are presented only for the core region. The theoretical values of the pitot pressures were calculated using the local Mach number, which is computed using an isentropic method-of-characteristics solution, to define the stagnation pressure ratio across a normal shock wave (p_{t2}/p_{t1}). The effect of the local flow inclination was not included in the calculation procedure. The effect on the

theoretical stagnation ratios presented in Fig. 6 should be small, since, as Pope and Goin[25] note, a pitot probe "will be insensitive to angle of attack up to 10 deg for an orifice diameter of only 10 percent of the outside diameter and up to 15 deg for one 98 percent of the outside diameter." The theoretical total-pressure distributions in the nozzle exit-plane are in very good with the experimentally-determined distributions. Referring to the tabulated values of Ref. 24, the total pressures indicate that the Mach number varies from 2.13 near the axis to 2.48 near the wall of the nozzle. Recall that if one assumes that the flow undergoes a one-dimensional acceleration from the sonic throat to the stream tube of the exit plane, the Mach number would be 2.36. Thus, although the C3 is a conical nozzle, the flow in the nozzle exit-plane is not conical.

For $x = 0.5\ r_{ne}$, the pitot-pressure measured in the internal region are in reasonable agreement with the theoretical values. The theoretical model even predicts the variation which occurs near $r = 0.5\ r_{ne}$. For $r > 0.965\ r_{ne}$, the measured pitot-pressures decrease rapidly with increasing r until near the plume boundary. These data illustrate that since the Mach number is constant along an "inviscid plume boundary", the local Mach number is a maximum at a point between the edge of the core region and the plume boundary.

When the stagnation pressure is $8.715 \times 10^6\ N/m^2$, the static pressure in the nozzle exit-plane is roughly six times the atmospheric value. Thus, as the exhaust gases leave the nozzle, they accelerate rapidly until the pressure along the plume boundary is equal to the static pressure of the surrounding gas. The plume boundaries for the C3 (20° conical) and for the C5 (10° contoured) nozzles, as calculated using the method-of-characteristics are presented in Fig. 7. The plume boundaries computed using the method-of-characteristics are in excellent agreement with those observed in the schlieren photographs of the nozzles exhausting into quiescent air. This is true for both of these nozzles, which are of considerably different geometries.

The correlation between the theoretical and the experimentally-determined flow-fields indicates that the nozzle-exhaust flow-field can be well modeled analytically. Thus, the method-of-characteristics for axisymmetric flow provides an acceptable tool even when no direct provisions are made for the occurence of internal shocks. As will be seen, the plume impingement and the initial wall-pressure rise will be described with sufficient accuracy by the method-of-characteristics followed by plane shock relations.

The internal radii of the launch tubes used in the present test program are from 1.2 r_{ne} to 1.5 r_{ne}, depending on the launch-tube configuration. Since the developing shear layer is relatively short, the ensuing viscous/shock-interaction structure at the wall is very dependent on the expansion process as the flow leaves the nozzle.

For the relatively small values of r_t/r_{ne} of interest in tube-launched-rocket applications, it is necessary to model the plume boundary only for a short distance. Thus, the calculation of the inviscid plume boundary by a technique which provides quick, but reasonable contours becomes attractive. The theoretical plume boundaries have been calculated using the method-of-centered-expansions[9,10]. These approximate plume boundaries are compared with those calculated using the more rigorous method-of-characteristics and with the data in Fig. 7. Note that the plume boundary calculated using the method-of-centered-expansions is very close to the actual boundary for both nozzles. However, at a given x-location, the local flow angle at the plume boundary calculated using the method-of-centered-expansions is slightly less than the actual flow angle. Thus, the inviscid plume boundaries calculated using the method-of-centered-expansions provide a close approximation of the actual plume boundaries, making the method attractive for use in generating quick calculations of the plume impingement flow.

Launch-Tube Flow Fields

When a highly underexpanded supersonic nozzle exhausts into a constant-area tube, the viscous/shock-wave interaction due to the impinging flow is subject to a boundary condition in the base region. If the annular gap between the rocket and the launch-tube wall is open, the atmospheric pressure at the forward end of the vented annular gap forms the boundary condition. The direction and the magnitude of the secondary flow which is usually generated by the impingement interaction is controlled by this boundary condition. If the mass flow-rate of the secondary flow in the annular gap is relatively low, the pressure will vary only slightly along the annular gap. Thus, the static pressure in the base region will be approximately equal to the atmospheric value. However, if the annular gap is sealed, the pressure in the base region will assume a value such that the viscous/shock-wave interaction at impingement creates a "constant-mass" recirculating flow in the base region.

Pressure distributions for the launch-tube flow-fields with the annular gap sealed by an obturator ring. - Over a wide range of stagnation pressure, the ratio p_b/p_{t1} is essentially independent of the stagnation pressure when the annular gap is sealed. That the pressure ratio p_b/p_{t1} should be constant for a given configuration for a fully developed supersonic flow is well documented, e.g., refs. 23, 26, and 27, Korst et al[28] have shown that the equilibrium (or steady-state) value of the base pressure is governed by the viscous shear-layer at the boundary of the nozzle exhaust plume that bounds the "dead-air" base-flow region and by the physical geometric constraints. The theoretical values of the base pressure are presented for the C3 and the C5 nozzles in Fig. 8 for all three launch tubes for stagnation pressures from 2.5×10^6 N/m^2 to 8.8×10^6 N/m^2.

The experimental values of the static wall-pressure vary only slightly with x in the region between the obturator ring (small negative x-coordinate) and the intersection of the exhaust plume with the launcher wall, reaching a minimum just before the impingement-induced pressure rise.

This is illustrated by the data presented in Figs. 9 and 10. For the purposes of the present paper, the static wall-pressure sensed by the orifice located at x = 0.0 r_{ne} (i.e., in the plane of the nozzle exit) is designated as the base pressure. The experimental values of p_b are presented in Fig. 8. Since they are a linear function of p_{t1}, the ratio p_b/p_{t1} is constant for a given configuration. Furthermore, they compare very well with the theoretical values for both nozzles.

The static-pressure distributions in the vicinity of the plume impingement have been computed for flows with the annular gap sealed by an obturator ring. The pressure distributions for unheated air accelerating from a reservoir where p_{t1} is 8.715 x 10^6 N/m^2 through the C3 nozzle into the constant-area launch-tubes are presented in Fig. 9. Similar solutions for the C5 nozzle are presented in Fig. 10. The theoretical solutions are compared with experimental data for these nozzle/launch-tube configurations. Note, that as the tube radius is increased from 1.20 r_{ne} (the L1 tube) to 1.50 r_{ne} (the L3 tube), the base pressure decreases and the location of the peak pressure moves further downstream of the nozzle exit-plane. However, as the base pressure decreases, the angle through which the plume boundary expands at the nozzle exit-plane increases. As a result, the pressure ratio across the impingement shock-wave (i.e., the peak static-pressure divided by the base value) increases as r_t increases.

For both nozzles, the theoretical value of the peak pressure in the impingement region is significantly greater than the corresponding experimental value for the L1 launch-tube. Because of the small difference between r_t and r_{ne}, the free-shear layer at the plume boundary is relatively short and the flow deceleration associated with the impingement process significantly modifies the viscous/shock-wave interaction. This modification is not reflected in the theoretical flow model, and thus, the peak pressure is overestimated by the theory. However, the agreement between the theoretical and the experimental values are much better for the L3 launch-tube. The improvement in the correlation for the larger-radius launch-tube is attributed to compensating effects of approximations in the theoretical flow model.

Pressure distributions for the launch-tube flow-fields with a vented annular gap. - As noted earlier, if the mass flow-rate of the secondary flow in the annular gap is relatively low, the pressure will vary only slightly along the annular gap. Since the static pressure in the nozzle exit-plane (p_{ne}) is directly proportional to the stagnation pressure, while the base pressure (p_b) remains roughly constant, the jet pressure ratio (p_{ne}/p_b) varies with p_{t1}. Thus, the viscous/shock-wave interaction depends on the stagnation pressures as well as the nozzle/launch-tube configuration.

The effect of the launch-tube radius is indicated by the pressure distributions presented in Figs. 11 and 12 for the largest value of p_{t1} tested. Since the base pressure is approximately constant, the shape of the plume boundary would be independent of the launch-tube radius, if the flow were inviscid. If the shape of the plume boundary were indeed independent of the launch-tube radius, as r_t decreased, the intersection of the plume boundary and the wall would be nearer the nozzle exit. Thus, the impingement shock-wave would move upstream and increase in strength as r_t decreases.

These trends are substantiated by both the theoretical and the experimental pressure distributions for the nozzle/launch-tube configurations using the C5 nozzle, which are presented in Fig. 12. As was the case for the flow fields with the obturator ring, the correlation between theory and experiment is better for the larger radius launch-tube, the L3. As before, the theoretical model of the shear layer does not reflect the interaction between the approaching free shear-layer and the pressure rise of the impingement shock-wave. However, as was shown in Fig. 7, the method-of-centered-expansions, which is used to provide the approximate inviscid plume boundary, yields plumes for which the local flow angle at the plume boundary is slightly less than the actual flow angle. Because these two flow-model approximations tend to compensate each other, the theoretical values of the peak pressure are in very good agreement with the data for these flow/geometry conditions.

Although experimental pressure distributions are presented for all three C3/launch-tube configurations, only for the C3/L3 is the theoretical distribution presented. Theoretical solutions were not possible for the C3/L1 or for the C3/L2 configurations with the present flow model, since the local flow inclination at the plume boundary intersection with the launcher wall exceeds the value which can be turned through a weak shock-wave. This contrasts the flow fields for the sealed annular gap. Recall that theoretical pressure distributions were presented in Fig. 9 for all three launch tubes when the annular gap was sealed by an obturator ring. As shown in Fig. 8a, the base pressure is considerably greater than the atmospheric value, when the annular gap is sealed, and the expanding flow turns through a smaller angle as it leaves the nozzle. Therefore, with an obturator ring in place, the local flow inclination of the impinging plume is such that the impingement shockwave is weak.

Although the theoretical solutions indicate the weak impingement shock-waves are not possible for the C3/L1 or the C3/L2 configurations, the maximum measured values of the pressure are not large enough to indicate the presence of a strong shock-wave. Thus, these pressure distributions indicate a relatively strong interaction between the impingement shock-wave and the free-shear at the plume boundary. For the two smaller radii tubes, the streamwise pressure-gradient along the launcher wall is not constant in the impingement region. As was discussed in ref. 23, the relatively strong viscous/shock-wave interaction which occurs for this nozzle/launch-tube configuration at high stagnation pressures produces significant blow-by flow.

Secondary flows. - As the rocket exhaust entrains base-region air, a free-shear layer develops along the plume boundary, accelerating air from the base-region and decelerating exhaust gas. When this free-shear layer encounters the adverse pressure gradient associated with the impingement shock-wave, some of the flow passes through the shock wave, some of it is turned back. As discussed in Fig. 1, if the stagnation pressure is relatively low, the system acts as an ejector with some of the entrained air passing through the impingement shock-wave. As the stagnation pressure

is increased, the ratio p_{ne}/p_b increases and the flow expands through a larger angle as it leaves the nozzle. As a result, the strength of the impingement shock increases. Once the impingement shock is sufficiently strong, the resultant adverse pressure gradient causes a fraction of the exhaust flow to be turned upstream (blow-by flow).

Theoretical and experimental values of the secondary flow rates are presented as a function of the stagnation pressure in Figs. 13 and 14. For all three configurations, theory provides a good prediction of the stagnation pressure for which there is no flow in the annular gap. However, the theory provides reasonable estimates of the secondary flow rates only for relatively low flow rates. This is evidenced by the comparison between data and theory for the C3/L3 configuration, which deteriorates as p_{t1} increases above 6×10^6 N/m^2.

This result should not be surprising. Furthermore, as has been often noted, the theoretical model of the shear-layer does not reflect the interaction between the approaching free shear layer and the pressure rise of the impingement shock-wave. Both of these approximations contribute to the limitation of the flow model to the prediction of the lower secondary flow rates. As the model is presently formulated, the secondary flows are only carried between streamlines within the linear mixing profile. Thus, the model is not applicable to high secondary flow-rates.

For the C5/L1 configuration, the theory provides a reasonable approximation of the crossover value of the stagnation pressure but does not come close to the blow-by flow-rates, as shown in Fig. 14. Part of the difference may be experimental. Since the diameter of the pitot probe was approximately 50 of the width of the annular gap for the L1 tube configuration, inaccuracies in the total pressure measured by the pitot probes may contribute to significant experimental errors. Nevertheless, the theoretical flow model provides a reasonable estimate of the stagnation pressure required for zero secondary flow.

Concluding Remarks

An engineering model has been developed to describe the impingement flow field which is produced when an underexpanded supersonic nozzle exhausts into a constant-area tube. Solutions of the theoretical flow-fields have been computed from the transonic region of the nozzle throat, through the nozzle, and through the impingement of the exhaust plume on the launcher wall. The theoretical solutions have been compared with experimental data. Based on the correlations between the data and the theory, the following conclusions are made.

1. The correlations between the theoretical and the experimentally-determined flow-fields in the nozzle and of the free exhaust plume indicate that the nozzle-exhaust flow-field can be well modeled analytically.

2. With the annular gap sealed by an obturator ring, the theoretical model closely predicts the static pressure in the "dead-air" base region. The theoretical and the experimental static wall-pressure distributions in the impingement region are in reasonable agreement, with the best correlation for the relatively large-radius tube.

3. For the vented annular-gap configurations, the theoretical wall-static pressure distributions in the impingement region again are in reasonable agreement with the data, providing the impingement shock-wave can be calculated using the weak, oblique, shock-wave relations.

4. The theoretical flow model provides a reasonable estimate of the reservoir (stagnation) pressure for which there is no secondary flow in the annular gap. However, the theoretical flow model represents the actual flow-field only when the secondary flow can be accommodated within the linear mixing profile.

References

1. J.J. Bertin, and J.L. Batson, "Comparison of Cold-Gas Simulations and Rocket-Launch Data for Constrictive Launchers," Journal of Spacecraft and Rockets, Vol. 13, No. 11, Nov. 1976, pp. 684-691.

2. H.H. Korst, T.L. Butler, and M.B. Briski, "Simulation of Jet Plume Interference Effects During the Launch Phase of Missiles", AIAA Paper No. 79-1292, presented at the AIAA/SAE/ASME 15th Joint Propulsion Conference, Las Vegas, June 1979.

3. _____: "Non-Tipoff Tube Launcher Flight Test Program," Report Number 7-52100/3R-61, LTV Aerospace Corp., Michigan Div., Dec. 1973.

4. W.H. Appich, Jr., and E.D. Tipping, "Free-Rocket Trajectory Errors from Plume-Induced Loading During Tube Launch," Journal of Spacecraft and Rockets, Vol. 14, No. 10, Oct. 1977, pp. 614-620.

5. D.W. Barnette, J.J. Bertin, and J.L. Batson, "Free-Flight Rocket's Initial Trajectory as Affected by Massive Blow-by", Journal of Spacecraft and Rockets, Vol. 15, No. 6, Nov.-Dec. 1978, pp. 334-340.

6. H.H. Korst, "A Theory for Base Pressures in Transonic and Supersonic Flow", Journal of Applied Mechanics, Vol. 23, 1956, pp. 593-600.

7. P. Carriere, M. Sirieix, and J. Delery, "Methodes de Calcul des Econlements Turbulents Decolks en Supersonique" Progress in the Aerospace Sciences, Pergamon Press, Vol. 16, No. 4, 1975, pp. 385-429.

8. P.M. Gerhart and H.H. Korst, "On the Free Shear Layer Downstream of a Backstep in Supersonic Flow", Journal of Fluids Engineering, ASME, Vol. 95, Series 1, No. 3, 1973, pp. 361-366.

9. N.H. Johannesen and R.F. Meyer, "Axially-Symmetrical Supersonic Flow Near the Centre of an Expansion", The Aeronautical Quarterly, Vol. 2, Aug. 1950, pp. 127-142.

10. H.H. Korst, "Analytical Concepts for the Modeling of Propulsive Jet Plume Interference Effects", UILU ENG 77-4010, Sept. 1977, The University of Illinois Experiment Station.

11. J.R. Kliegel and J.N. Levine, "Transonic Flow in Small Throat Radius of Curvature Nozzles", AIAA Journal, Vol. 7, No. 7, July 1969, pp. 1375-1378.

12. H.H. Korst and R.A. Deep, "Modeling of Plume Induced Interference Problems in Missile Aerodynamics", AIAA Paper No. 79-0362, presented at the 17th Aerospace Sciences Meeting, New Orleans, Jan. 1979.

13. R.A. White, "Effect of Sudden Expansions or Compressions on a Turbulent Boundary Layer ", AIAA Journal, Vol. 4, No. 12, Dec. 1966, pp. 2232-2234.

14. H.H. Korst and W.L. Chow, "Non-Isoenergetic Turbulent (Pr_t = 1) Jet Mixing Between Two Compressible Streams at Constant Pressure", CR-419, Apr. 1966, NASA.

15. H.H. Korst and W.L. Chow, "On the Correlation of Analytical and Experimental Free Shear Layer Similarity Profiles by Spread Rate Parameters", Journal of Basic Engineering, Trans. ASME, Series D, Vol. 93, 1971, pp. 377-382.

16. W. Tripp and H.H. Korst, "The Pressure on a Blunt Trailing Edge Separating Two Supersonic Two-Dimensional Air Streams of Different Mach Numbers and Stagnation Pressures, but Identical Stagnation Temperatures", Proceedings, 5th Midwestern Conference on Fluid Mechanics, University of Michigan, Ann Arbor, 1967.

17. R.H. Page, W.G. Hill, and T.J. Kessler, "Reattachment of Two-Dimensional Supersonic Turbulent Flow", ASME Paper 67-FE-20, 1967.

18. D.R. Bartz, "Turbulent Boundary Layers in Cooled, Convergent-Divergent Nozzles, ASME Transactions, Vol. 75, pp. 1235-1245, 1955.

19. H.H. Korst, "Effect of Turbulent Boundary Layer in Cooled C-D Nozzles on Plume Modeling", Final Report for Task Order 76-207, University of Illinois at Urbana-Champaign, Feb. 1976.

20. T.L. Butler, "Simulation of Jet Plume Interference in Gases of Dissimilar Specific Heat Ratio", M.S. Thesis, Department of Mechanical and Industrial Engineering, University of Illinois at Urbana-Champaign, 1976.

21. R.H. Page and V. Sernas, "Apparent Reverse Transition in an Expansion Fan", AIAA Journal, Vol. 8, No. 1, Jan. 1970, pp. 189-190.

22. J.J. Bertin, S.J. Sutter, Jr., D.P. Dannemiller, and D.L. Booker, "A Comparison of Theoretical and Experimental Flow Fields for an Underexpanded Rocket Exhaust", AIAA Paper 79-0340, presented at the 17th Aerospace Sciences Meeting, New Orleans, Jan. 1979.

23. J.J. Bertin, E.S. Idar, and D.L. Booker, "Secondary Flows for a Tube-Launched Rocket Configuration", AIAA Paper 80-0372 presented at the 18th Aerospace Sciences Meeting, Pasadena, Ca., Jan. 1980.

24. _____, "Equations, Tables, and Charts for Compressible Flow", Report 1135, 1953, NACA.

25. A. Pope and K.L. Goin, High-Speed Wind Tunnel Testing, J. Wiley and Sons, 1965, New York.

26. J. Fabri and R. Seistrunck, "Supersonic Air Ejectors", Advances in Applied Mechanics, Vol. V, Academic Press, Inc., 1958, New York, pp. 1-34.

27. R.C. German, R.C. Bauer, and J.H. Panesci, "Methods for Determining the Performance of Ejector-Diffuser Systems", Journal of Spacecraft and Rockets, Vol. 3, No. 2, Feb. 1966, 193-200.

28. H.H. Korst, W.L. Chow, and G.W. Zumwalt "Research on Transonic and Supersonic Flow of a Real Fluid at Abrupt Increases in Cross-Section (With Special Consideration of Base Drag Problems) -- Final Report", Report No. ME-TN-392-5, Dec. 1959, The University of Illinois.

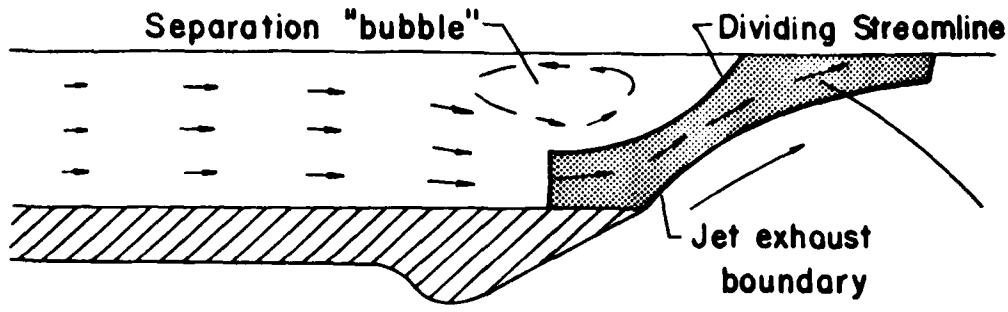

Launcher centerline

Shaded region designates air entrained from the base region which is given sufficient momentum to pass through the impingement shock wave.

(a) System acts as an ejector

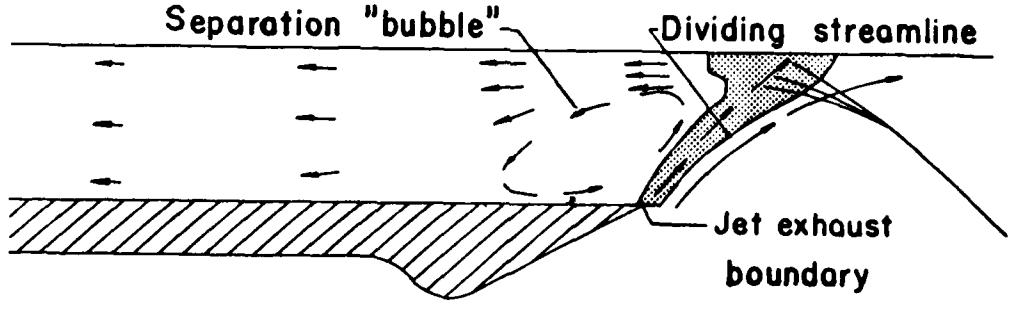

Launcher centerline

Shaded region designates that fraction of the exhaust flow which does not have sufficient momentum to pass through the impingement shock wave.

(b) System produces nominal blow-by flow

Figure 1. - Sketch of launch tube flow-fields that produce relatively small secondary-flow-rates.

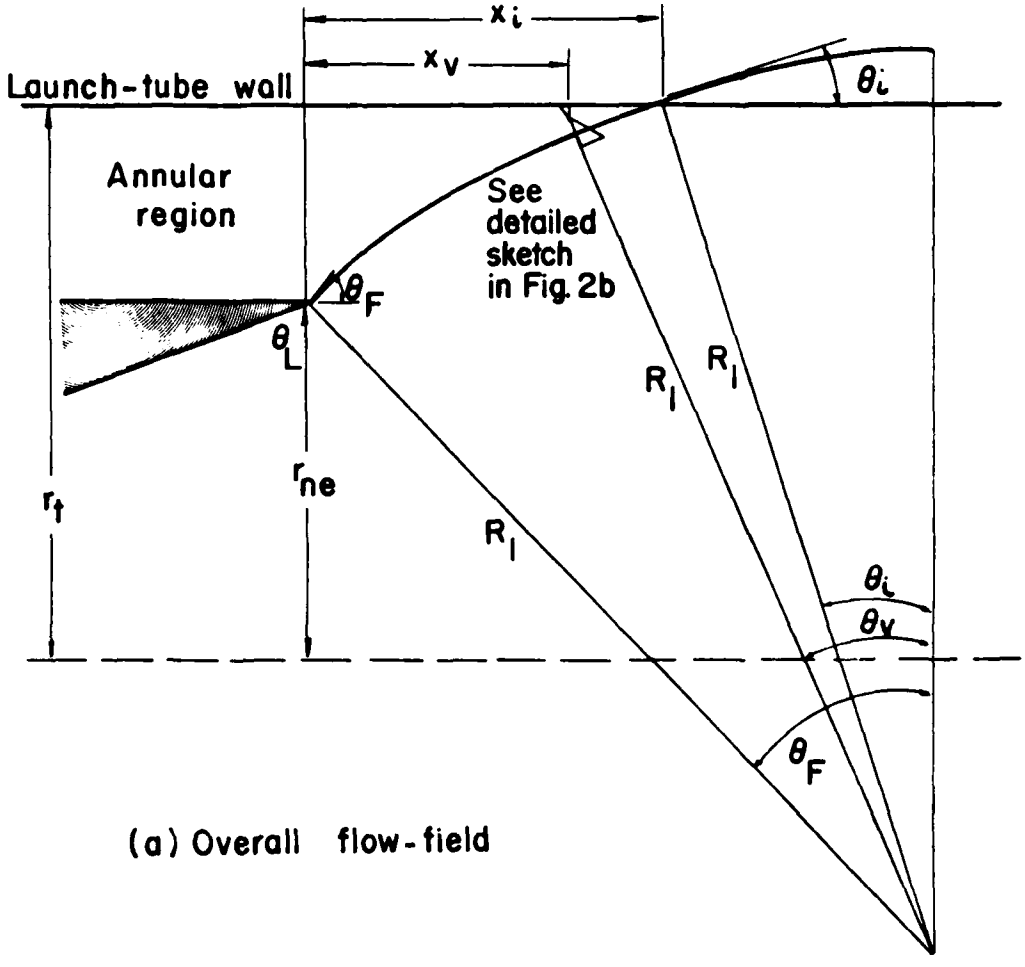

Figure 2. - Sketch of impingement flow.

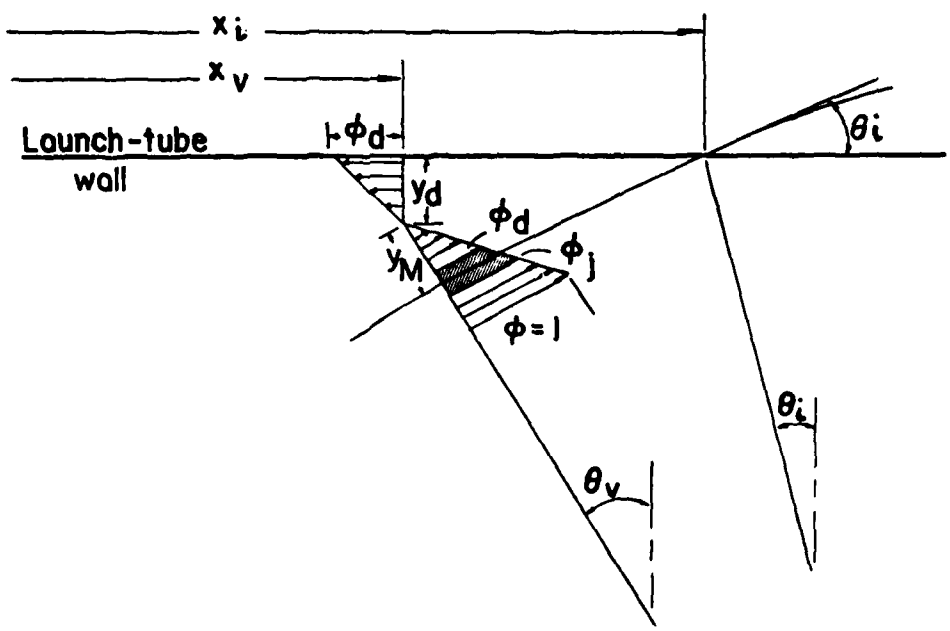

(b) Details of impinging shear-layer for ejector-type flow ($\phi_i > \phi_d$, ■ secondary flow)

Figure 2. - Concluded.

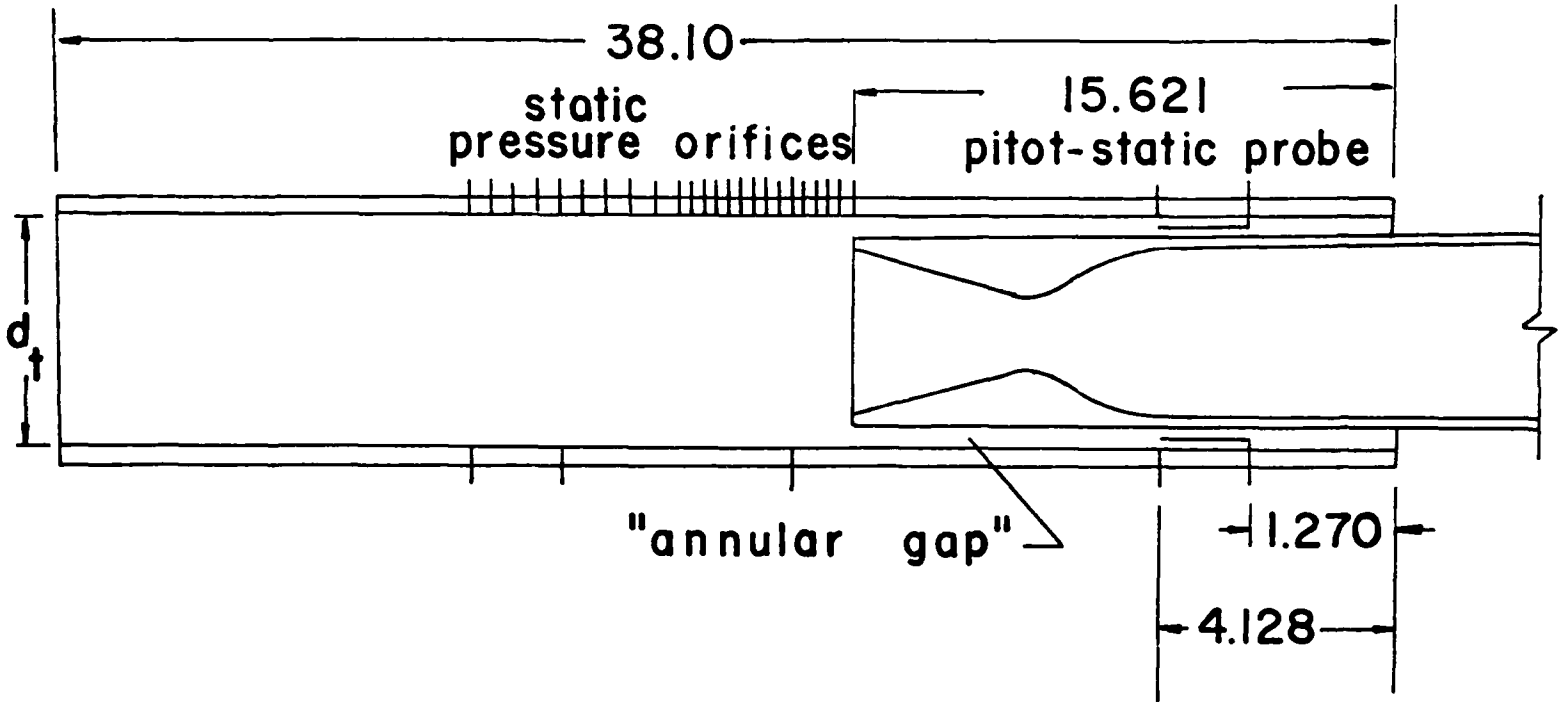

Figure 3. - Sketch of a typical nozzle/launch-tube configuration.

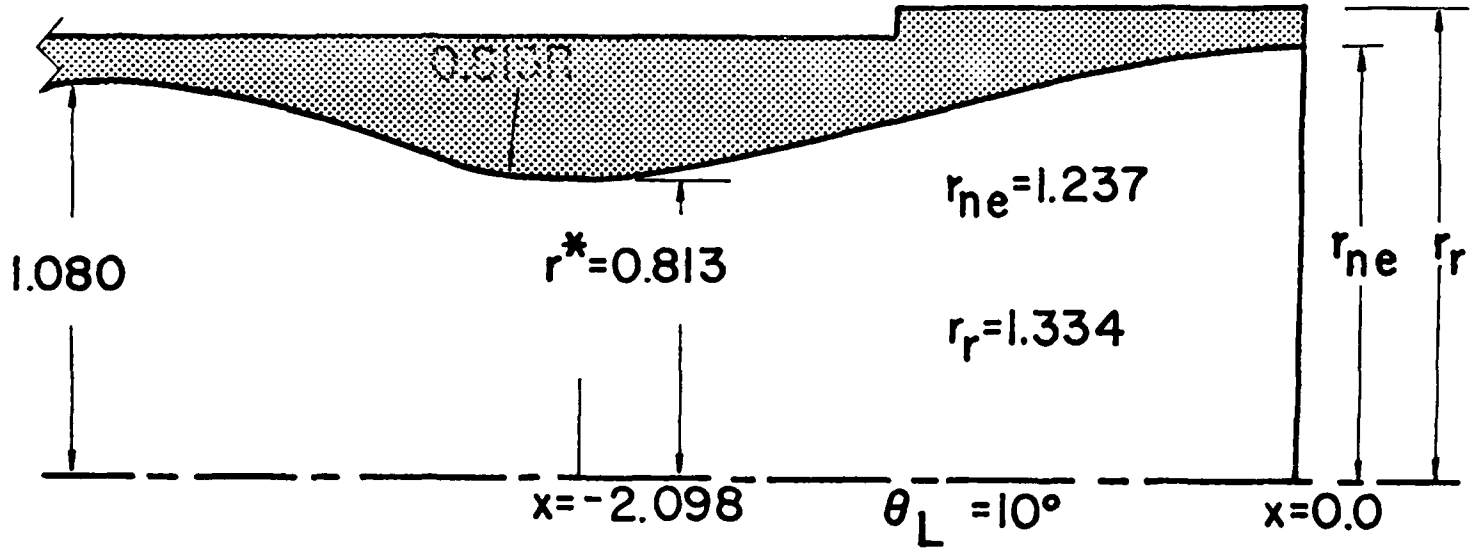

Figure 4. - Sketch of the C5 nozzle.

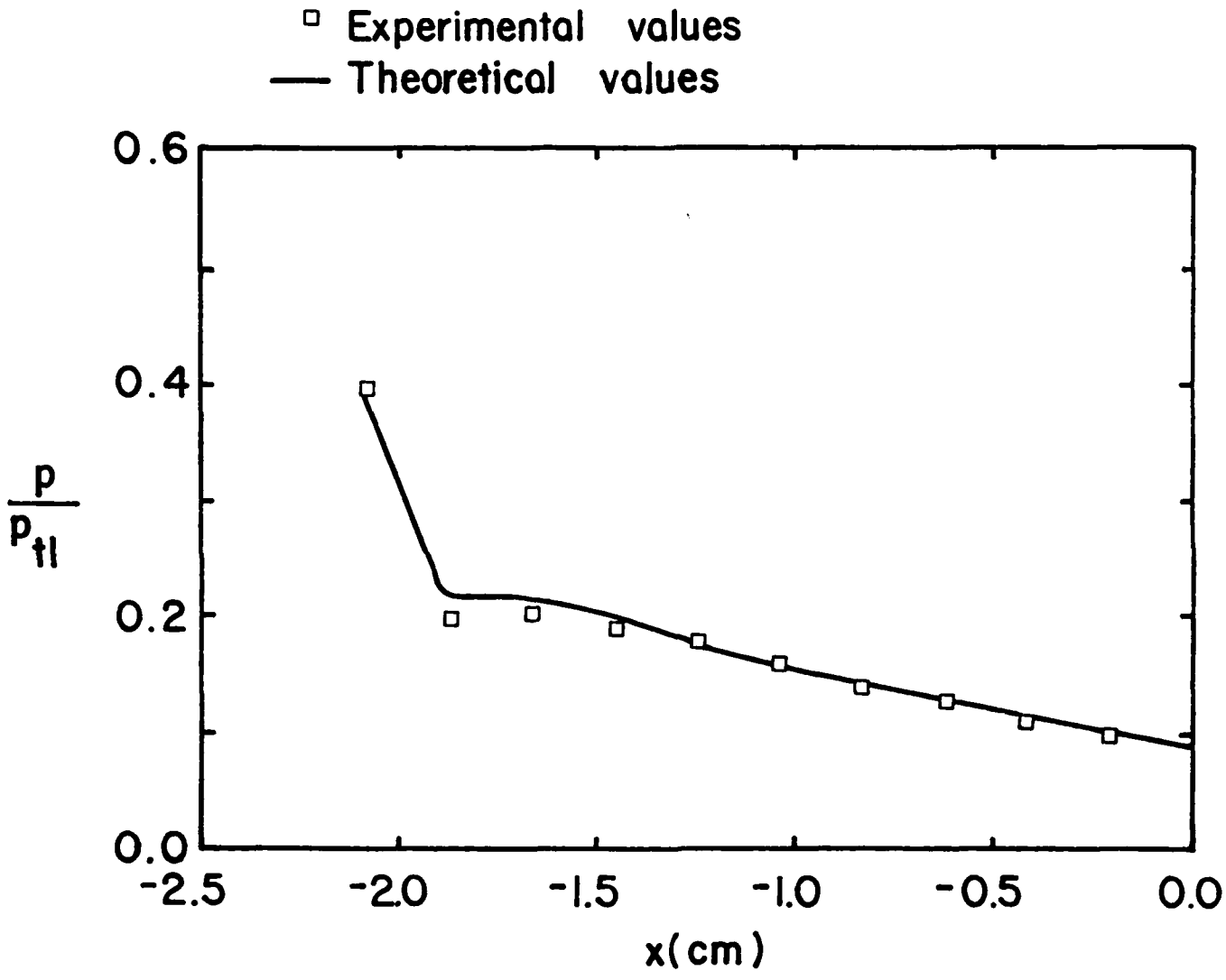

Figure 5. - Sketch of the static pressure distribution for the divergent section of the C5 nozzle.

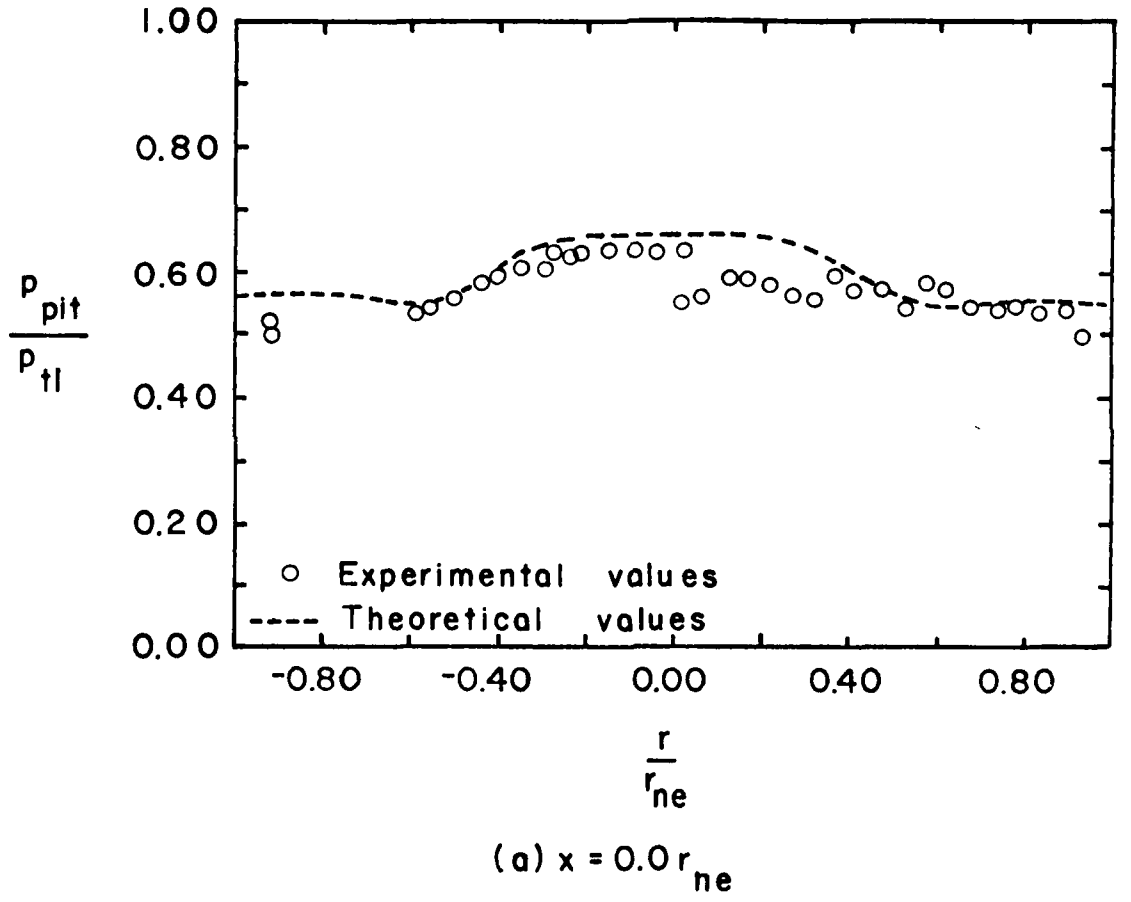

Figure 6. - Radial pitot-pressure distributions for the exhaust of the C3 nozzle ($p_{t1} = 8.715 \times 10^6$ N/m^2).

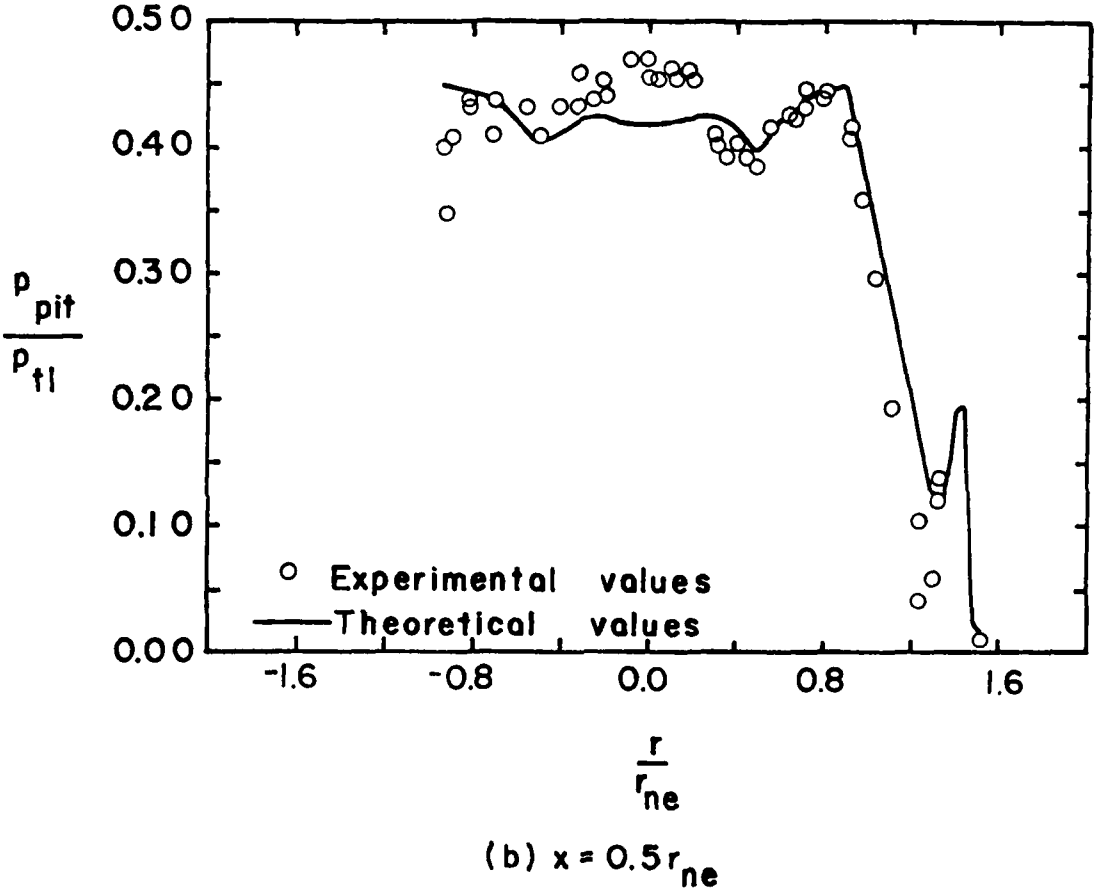

(b) $x = 0.5 r_{ne}$

Figure 6. - Concluded.

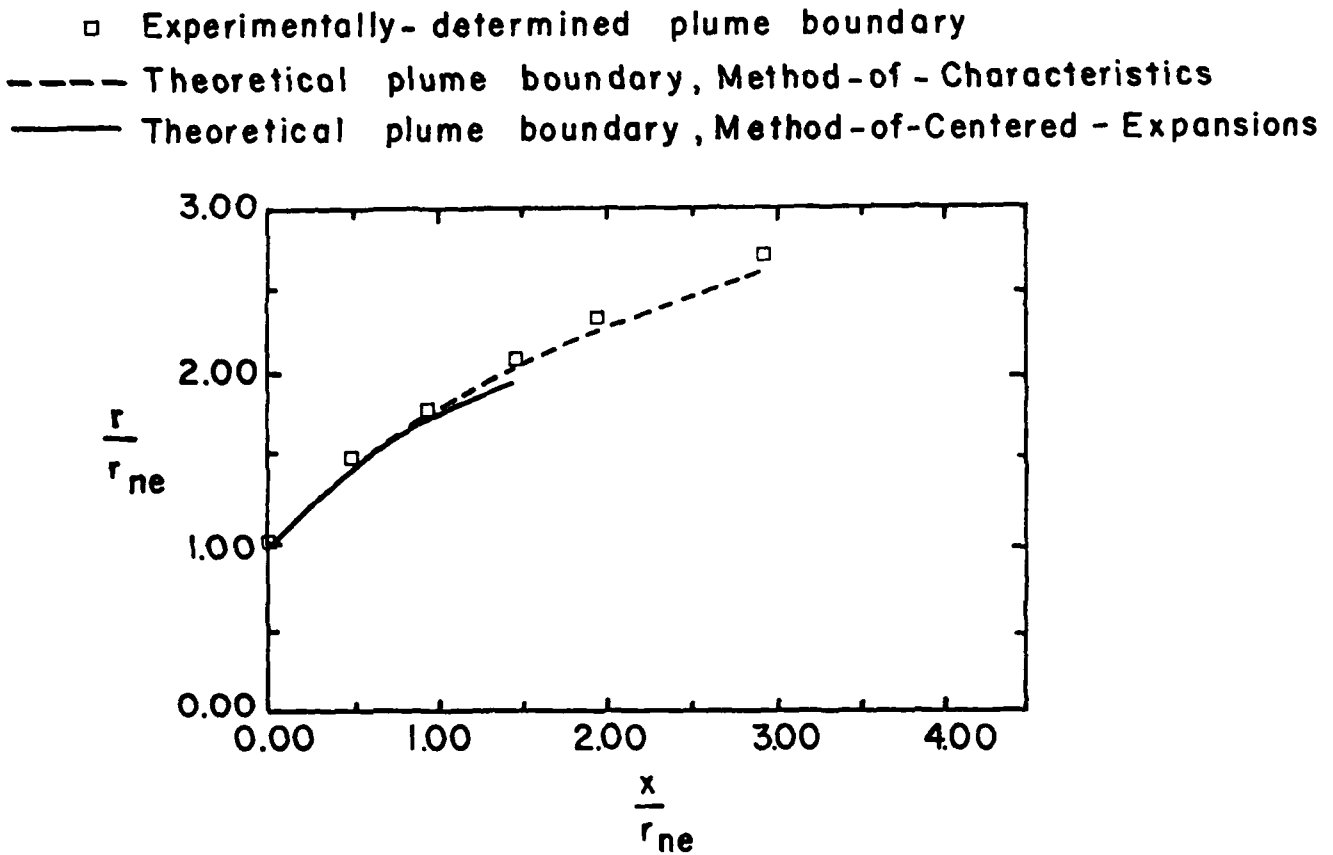

(a) C-3 Nozzle

Figure 7. - Plume boundaries for the C3 and for the C5 nozzles exhausting into quiescent air ($p_{t1} = 8.715 \times 10^6$ N/m^2).

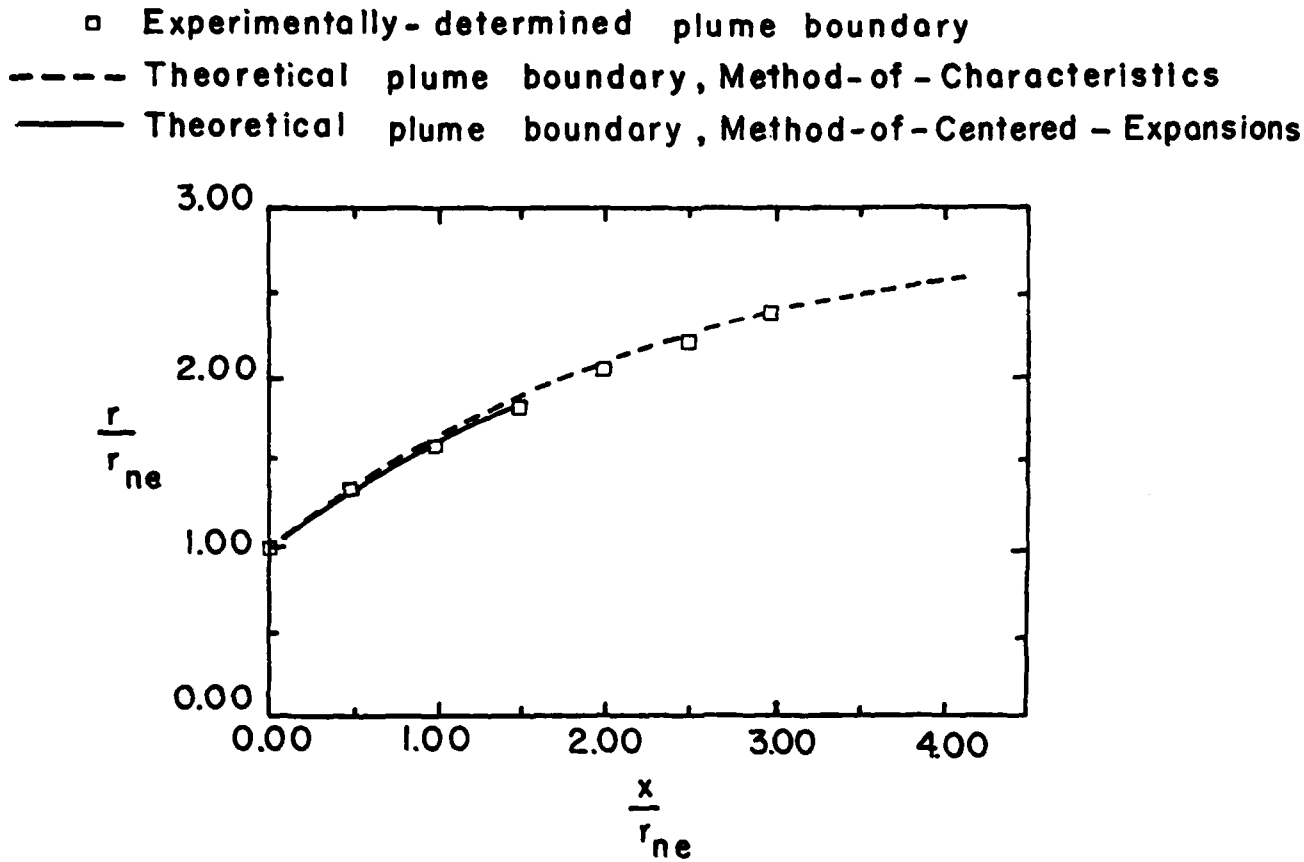

(b) C-5 Nozzle

Figure 7. - Concluded.

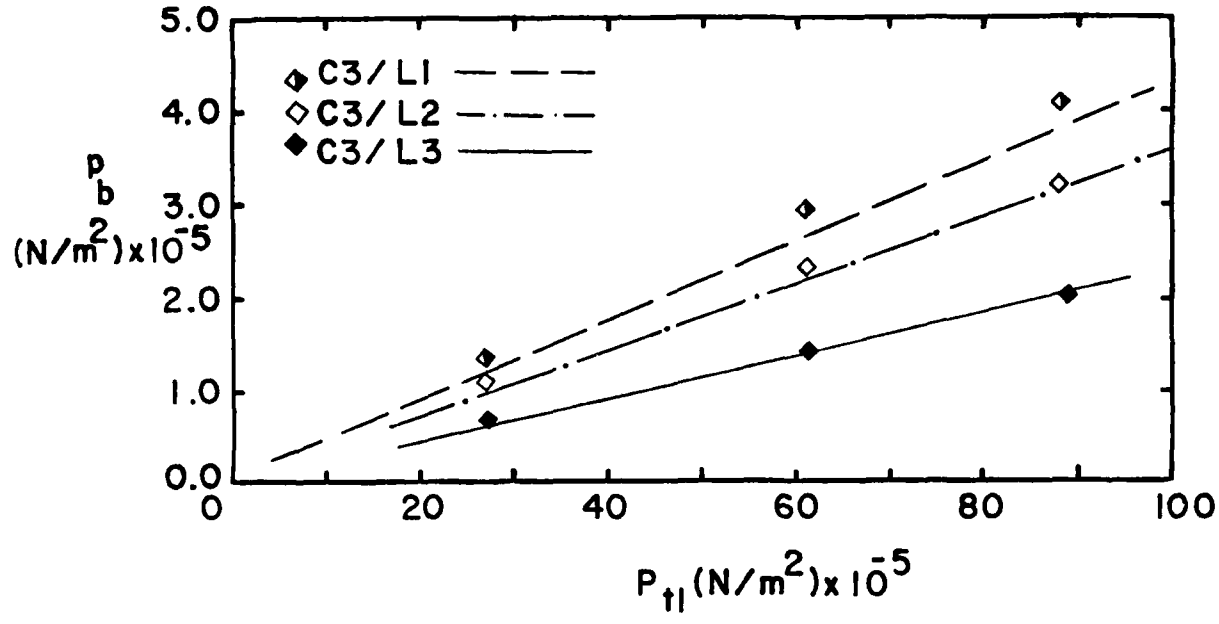

(a) C3 Nozzle

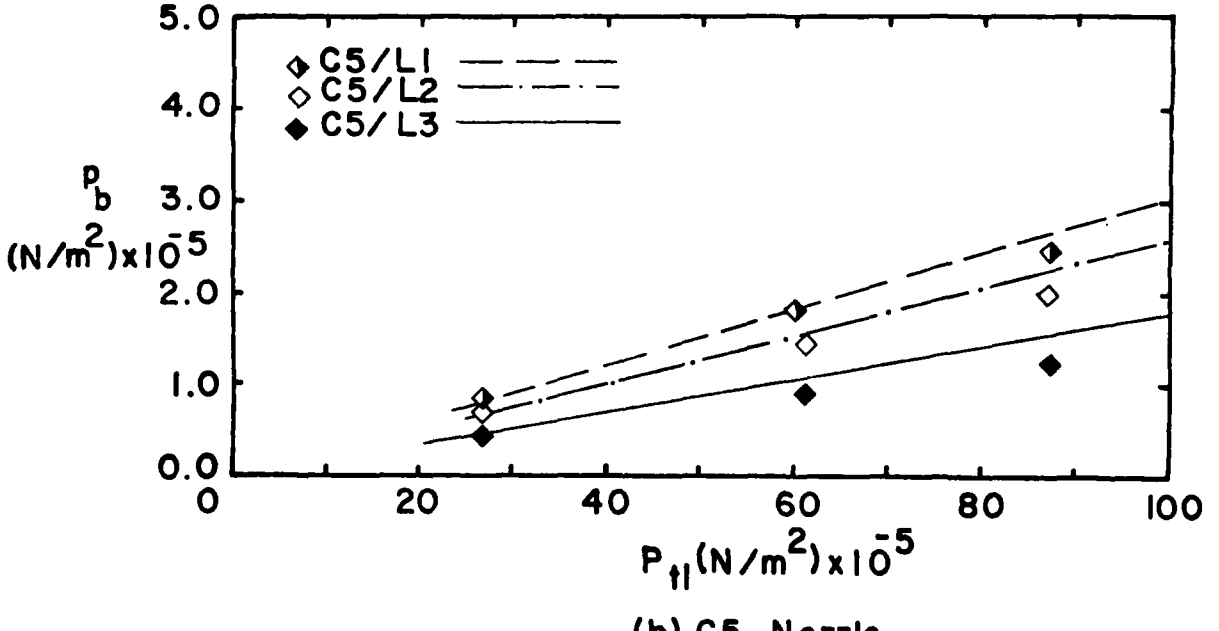

(b) C5 Nozzle

Figure 8. - Base region pressure for a sealed annular gap.

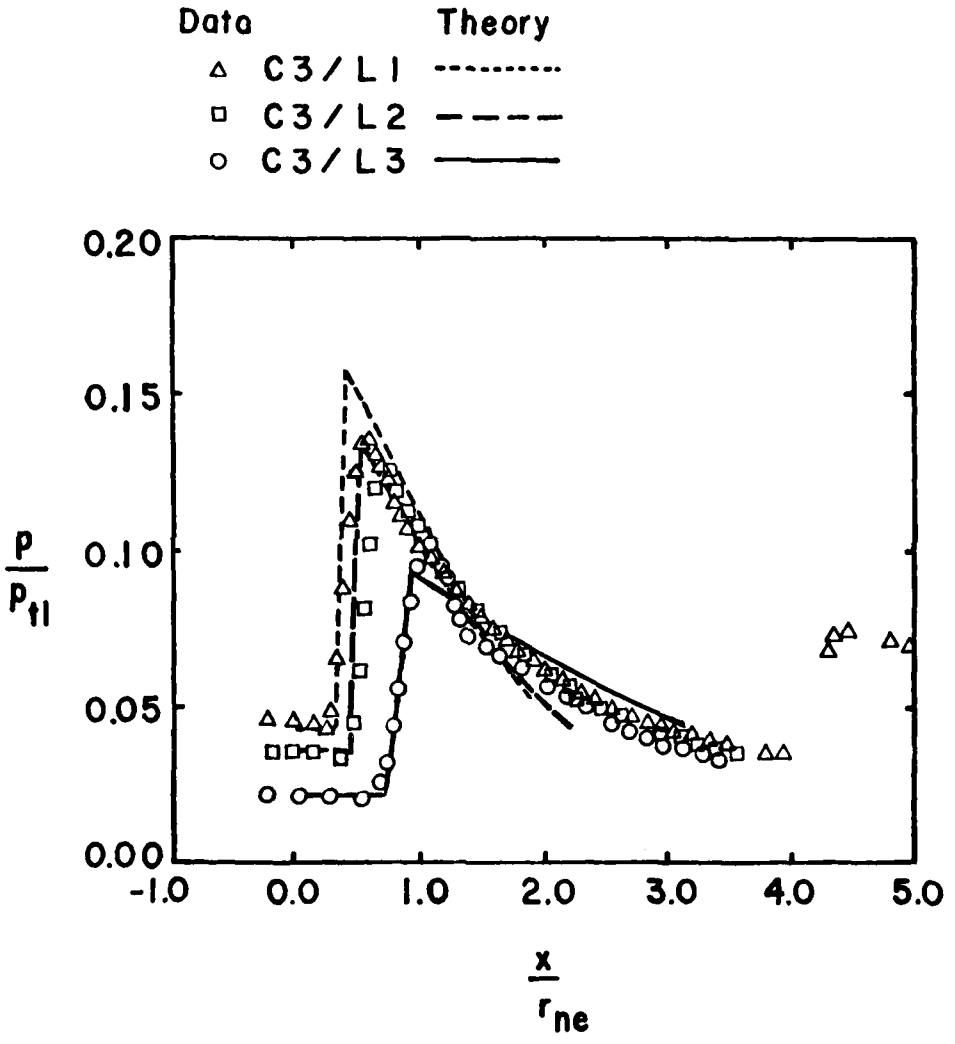

Figure 9. - Static-wall pressure-distributions for C3 nozzle exhausting into a launch tube with a sealed annular gap (p_{t1} = 8.715 x 10^6 N/m^2).

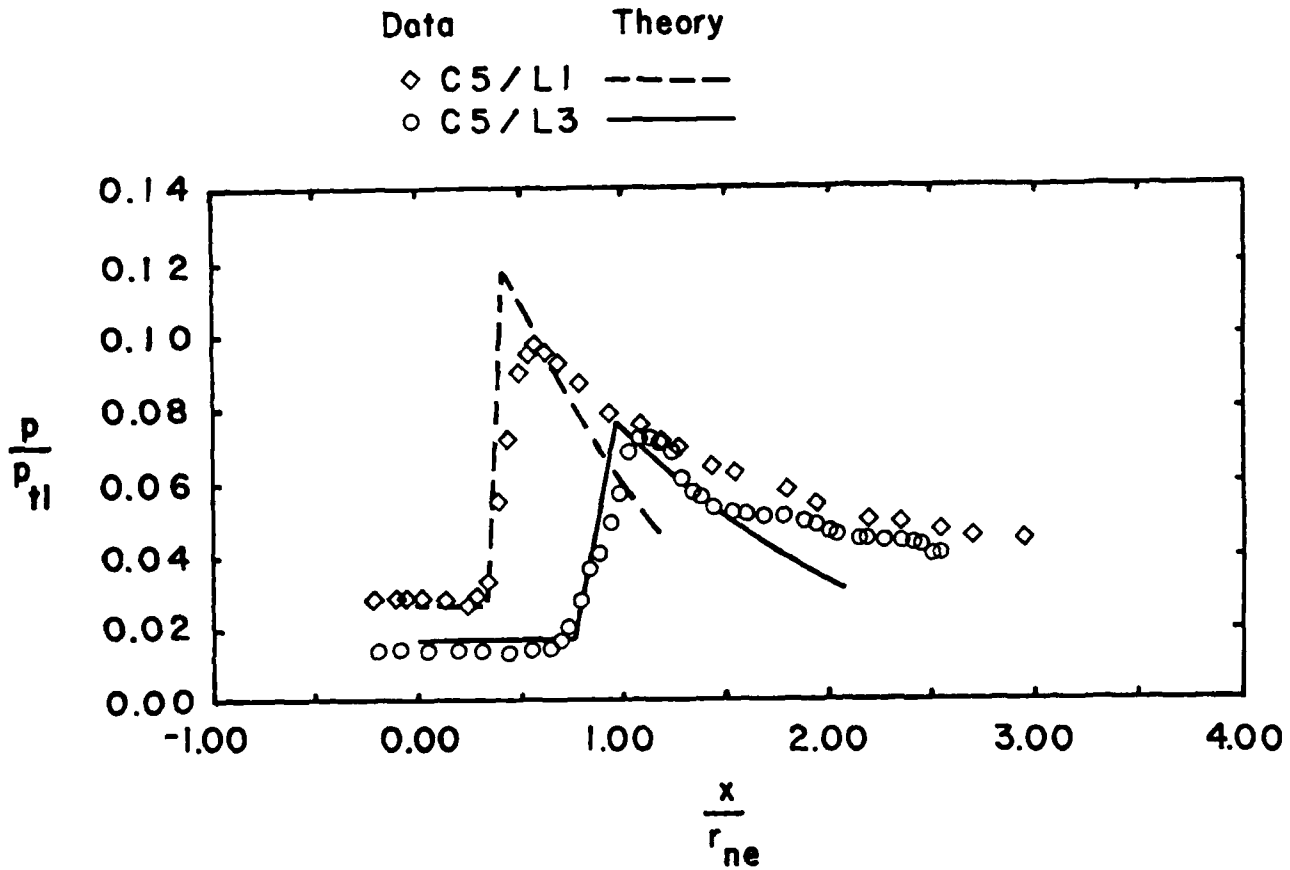

Figure 10. - Static wall-pressure-distributions for C5 nozzle exhausting into a launch tube with a sealed annular gap (p_{t1} = 8.715 x 10^6 N/m^2).

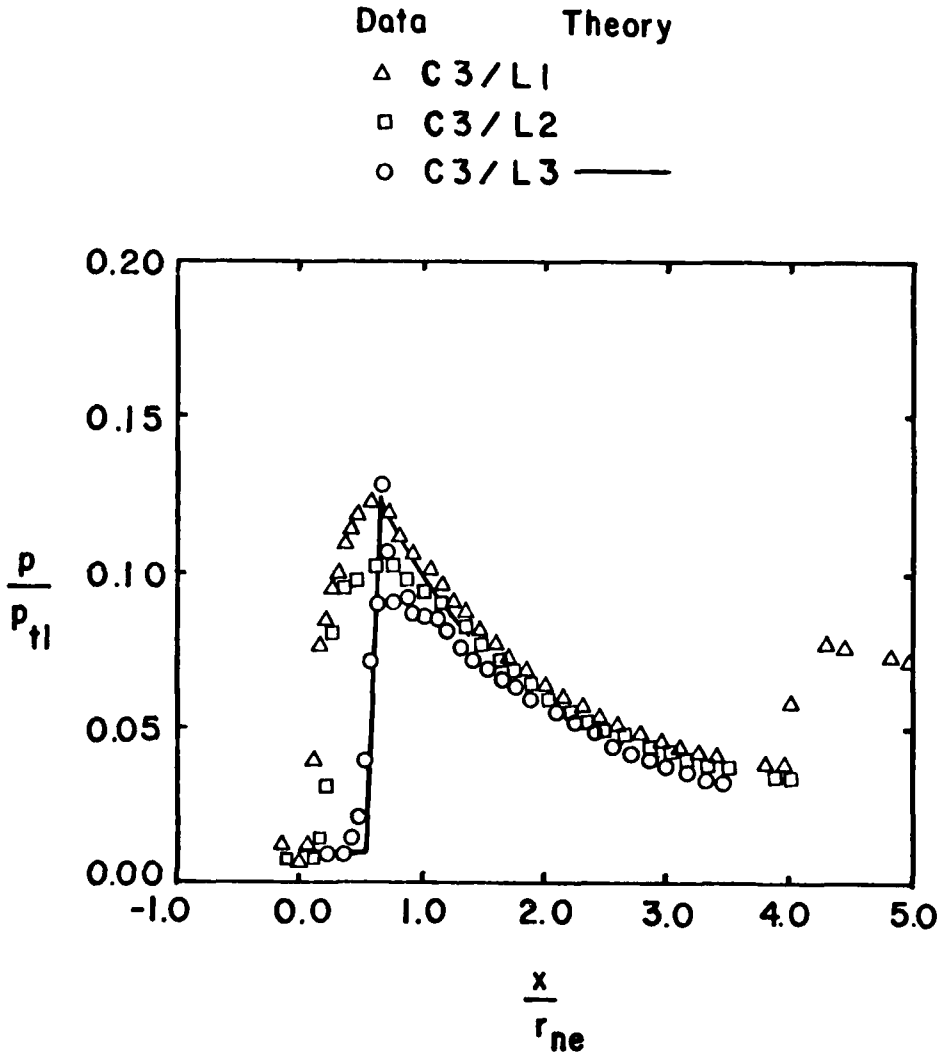

Figure 11. - Static wall-pressure-distributions for C3 nozzle exhausting into a launch tube with a vented annular gap (8.715×10^6 N/m^2).

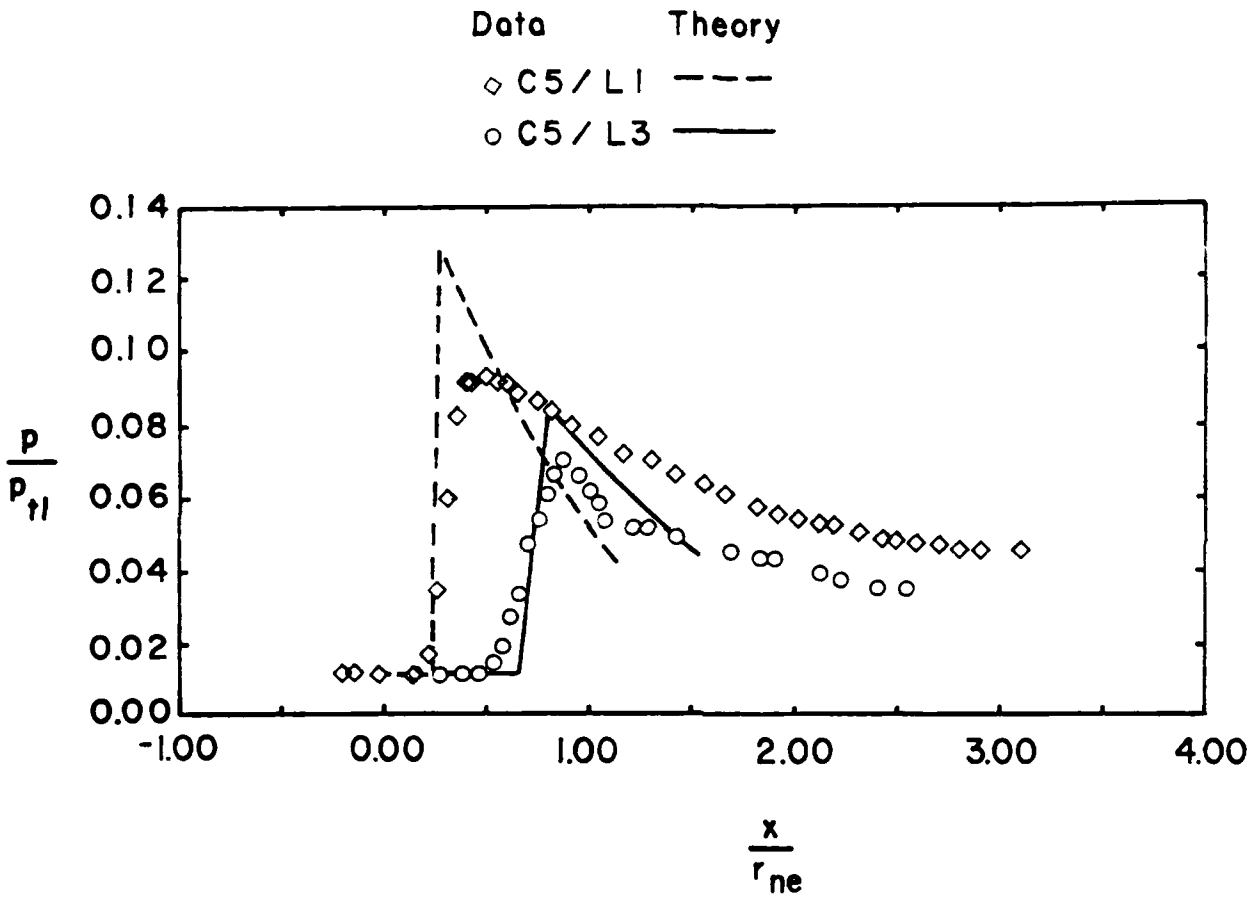

Figure 12. - Static wall-pressure-distributions for C5 nozzle exhausting into a launch tube with a vented annular gap ($p_{t1} = 8.715 \times 10^6$ N/m^2).

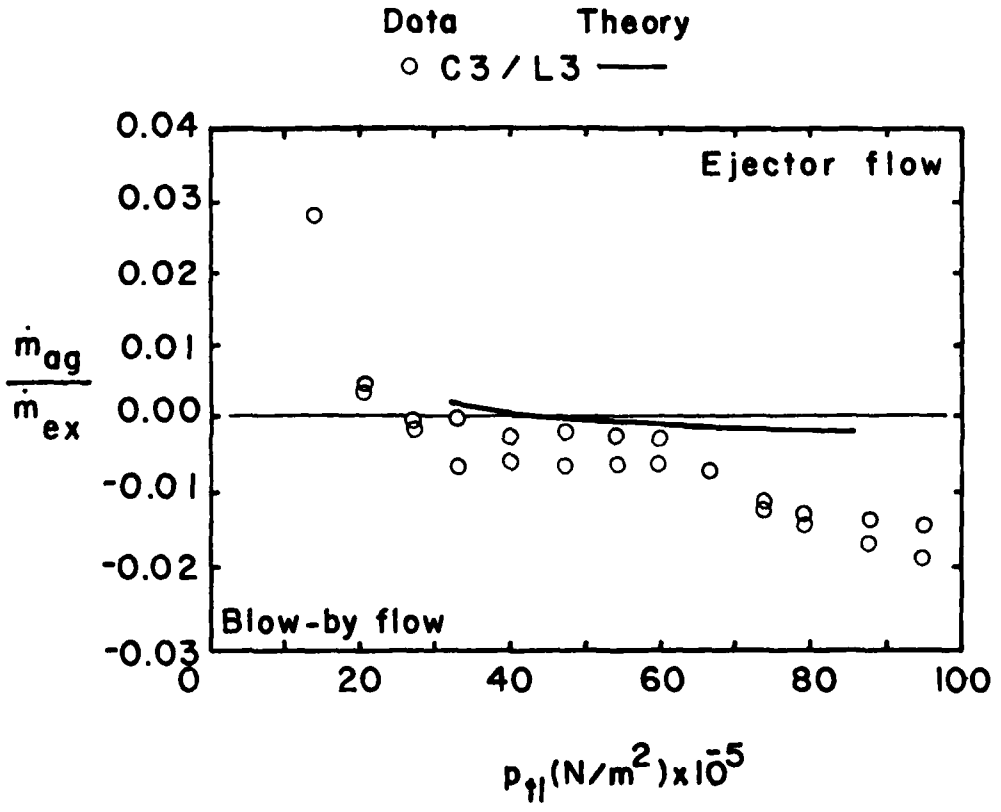

Figure 13. - Secondary-flow rates for the C3 nozzle exhausting into the L3 launch-tube with a vented annular gap.

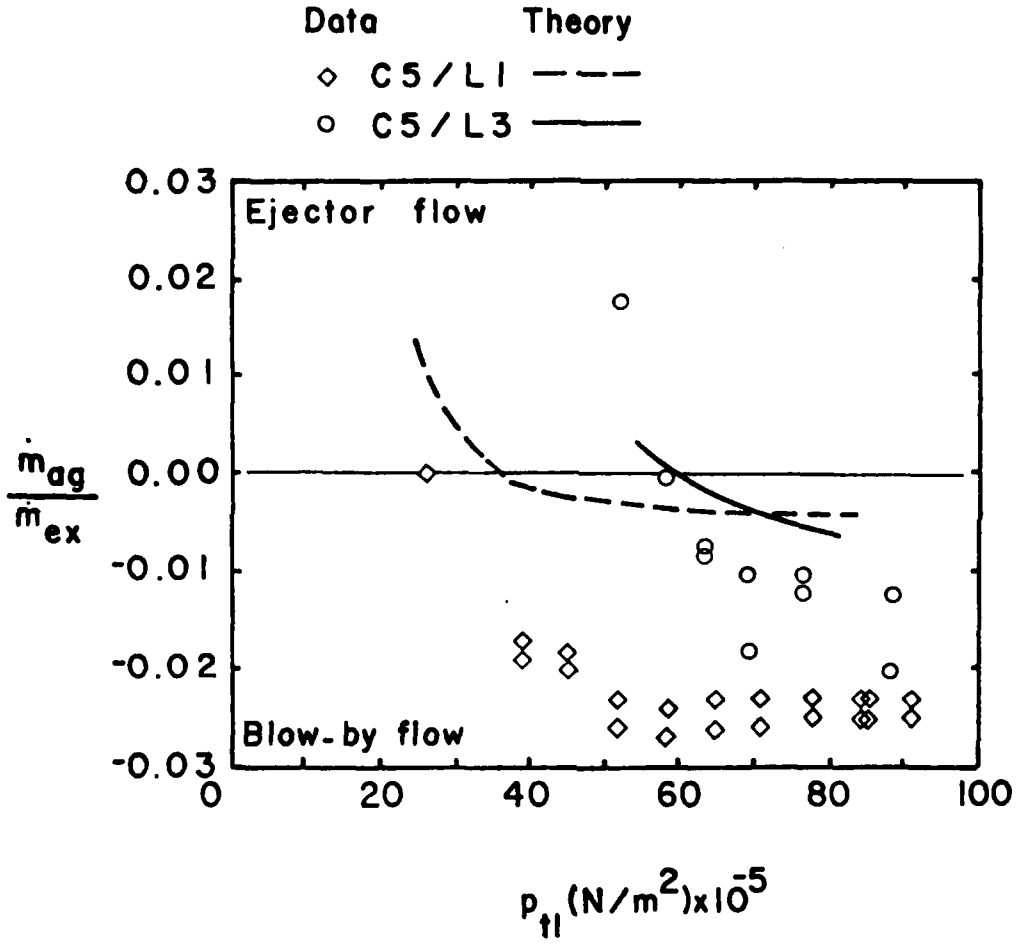

Figure 14. - Secondary-flow rates for the C5 nozzle exhausting into the L1 or the L3 launch-tube with a vented annular gap.

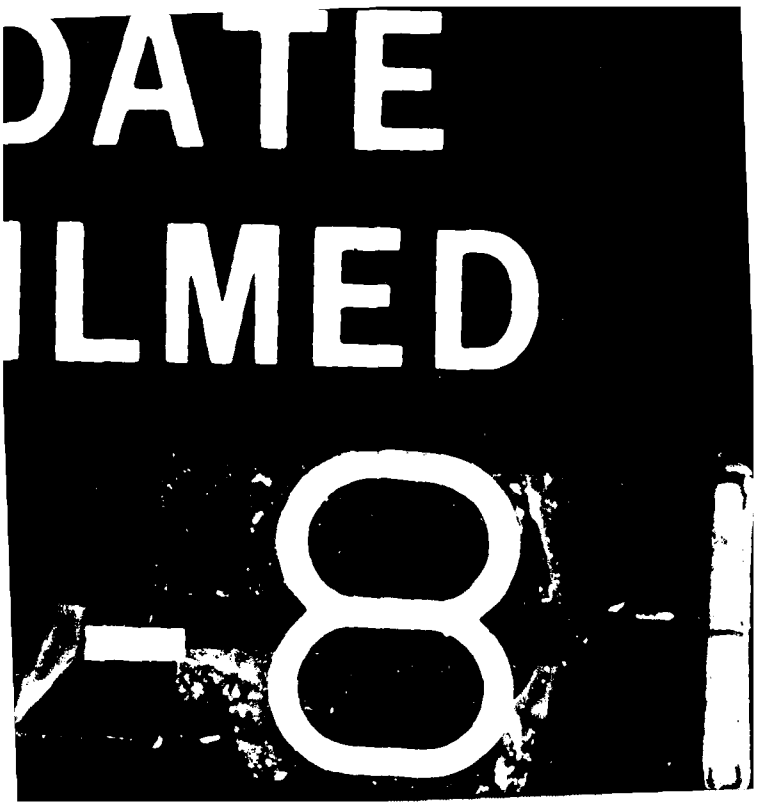
DATE
ILMED
-8